Advances in Water Resources xxx (2012) xxx–xxx

Contents lists available at SciVerse ScienceDirect

Advances in Water Resources

journal homepage: www.elsevier.com/locate/advwatres

A comparison of 1701 snow models using observations from an alpine site

Richard Essery [a,*], Samuel Morin [b], Yves Lejeune [b], Cécile B Ménard [c]

[a] School of GeoSciences, University of Edinburgh, Edinburgh EH9 3JW, UK
[b] Météo-France/CNRS, CNRM – GAME URA 1357, CEN, St. Martin-d'Hères, France
[c] Arctic Research Centre, Finnish Meteorological Institute, Helsinki, Finland

ARTICLE INFO

Article history:
Available online xxxx

Keywords:
Snow modelling
Ensemble modelling
Model selection
Snow processes

ABSTRACT

There are many models that attempt to predict physical processes in snow on the ground for a range of applications, and evaluations of these models show that they have a wide range of behaviours. A review of snow models, however, shows that many of them draw on a relatively small number of process parameterizations combined in different configurations and using different parameter values. A single model that combines existing parameterizations of differing complexity in many different configurations to generate large ensembles of simulations is presented here. The model is driven and evaluated with data from four winters at an alpine site in France. Consideration of errors in simulations of snow mass, snow depth, albedo and surface temperature show that there is no "best" model, but there is a group of model configurations that give consistently good results, another group that give consistently poor results, and many configurations that give good results in some cases and poor results in others. There is no clear link between model complexity and performance, but the most consistent results come from configurations that have prognostic representations of snow density and albedo and that take some account of storage and refreezing of liquid water within the snow.

1. Introduction

Amongst other applications, models of physical processes in snow on the ground are used in hydrological forecasting, numerical weather prediction and climate modelling. Papers describing the development of new snow models or improvements to existing models usually include comparisons of model predictions with observations (e.g. [3,6,16,32,34,99]). Other studies have contrasted the performance of several models at a time (e.g. [10,36,44]), and there have been a few major intercomparison projects evaluating snow simulations by large numbers of models (e.g. [13,42,90,95]). The organizers of such projects generally state that their aim is not to identify a "best" model but rather to relate differences in model behaviour to differences in model structure. Even this better-defined aim is hard to achieve in intercomparison projects because of complex interactions between the components within models and differing choices between models for the values of parameters that are often not well constrained [20]. As an alternative approach, this paper uses a single model with several options for the representation of each process considered to be important; the options are combined in every possible configuration to give a large ensemble of simulations with different model structures. Although it is taken to an unprecedented level here, the same philosophy underlies the Chameleon Surface Model (CHASM) [84], the Cold Region Hydrological Model (CRHM) [85], the Framework for Understanding Structural Errors in hydrological models (FUSE) [18], the multi-parameterization version of the Noah land surface model (Noah-MP) [78] and, more generally, the method of multiple working hypotheses for hydrological modelling advocated by Clark et al. [20]. Multi-model and perturbed model ensembles are now widely used in environmental modelling; ensemble means are often thought to provide more reliable predictions than single model realizations and ensemble spread is often taken as a measure of uncertainty in predictions [9,48,51].

Many snow models and land-surface models with snow modules are in use, and there are many papers describing them; models that will be referred to frequently in this paper are listed in Table 1. Reading a large number of documentation papers reveals that a small number of parameterizations are used time and time again in different combinations in different models, so the models are not all truly independent. The parameterizations of snow compaction introduced by Anderson [3] and Verseghy [104] are each used in several later models, for example. Many of the more physically-based models reference papers from the 1970s by Colbeck [22] and Anderson [3], although in fact they mostly adopt parameterizations from those papers as implemented in SNTHERM [60]. Our expectation is that a model with options covering the range of complexities currently used in representing particular processes will span the range of behaviours found in current models and will

* Corresponding author.
E-mail address: Richard.Essery@ed.ac.uk (R. Essery).

0309-1708/$ - see front matter © 2012 Published by Elsevier Ltd.
http://dx.doi.org/10.1016/j.advwatres.2012.07.013

Table 1
Example models.

BASE	Slater et al. [94]
BATS	Yang et al. [111]
CLASS	Verseghy [104]
CLM	Oleson et al. [80]
COUP	Gustafsson et al. [54]
Crocus	Vionnet et al. [105]
HTESSEL	Dutra et al. [34]
IAP94	Dai and Zeng [26]
ISBA-ES	Boone [11]
ISBA-FR	Douville et al. [32]
JULES	Best et al. [8]
MAPS	Smirnova et al. [96]
MATSIRO	Takata et al. [101]
MOSES	Cox et al. [23]
Noah-MP	Niu et al. [78]
SAST	Sun et al. [99]
SiB	Sellers et al. [92]
SNOBAL	Marks et al. [70]
SNOWPACK	Bartelt and Lehning [6]
SNTHERM	Jordan [60]
SPONSOR	Shmakin [93]
SSiB	Xue et al. [109]
SWAP	Gusev and Nasonova [53]
VIC	Andreadis et al. [4]
VISA	Yang and Niu [112]

make those behaviours easier to understand. The ensemble is not expected to span the full range of snow behaviours found in nature, however; redistribution of snow by wind and interactions with vegetation are important in many places but are not considered in the model used here. The model was first developed to investigate snow process parameterizations for the JULES community land surface model [8] and so is named the JULES Investigation Model (JIM) [103].

Conclusions from intercomparison projects relevant to this study are briefly reviewed in Section 2. Data used here for model driving and evaluation over four winters at one site are discussed in Section 3, and options for representing snow processes are described in Section 4. Simulations of particular processes in isolation from the rest of the model are compared with observations where possible before results from the full ensemble of simulations are presented in Section 5 and compared with observations in Section 6.

2. Snow model intercomparisons

At least five intercomparison projects have specifically considered snow processes or regions with significant seasonal snow cover: PILPS2d [91,95], PILPS2e [13,76], Rhône-AGG [12], SnowMIP [38,42] and SnowMIP2 [41,90]. More than 50 models have participated in one or more of these projects, and six models (CLASS, ISBA, MOSES, SPONSOR, SSiB and SWAP) have participated in all five. Snow processes have also been considered in global simulations compared by the Atmospheric Model Intercomparison Project [49], the Global Soil Wetness Project [30] and the Water Model Intercomparison Project [55].

Despite overlap in parameterizations and close family relationships between some models, intercomparison studies have shown that models differ greatly in their predictions of snow accumulation and ablation. As an example, Fig. 1 shows observations and simulations of snow mass at the four sites used in SnowMIP [38,42]. The spread among the 23 participating models increases when snow is melting, either during the winter or in spring, so simulation of snow is more challenging for warmer sites where mid-winter melt events are more likely. Some models took total precipitation as an input and used their own methods to partition it into snowfall and rainfall amounts differing from those provided in the driving data; this is particularly apparent for two of the Col de Porte simulations. Errors in simulations of net shortwave radiation were larger than errors in net longwave radiation and did not appear to be strongly influenced by model complexity. In some cases, models that simulated snow melt well had poor simulations of snow albedo.

Thirty-three models performed simulations for five pairs of open and forested sites in SnowMIP2 [41,90]. The duration of snow cover was generally predicted well, but there was a broad range in simulations of maximum snow mass, particularly at warmer sites and in warmer winters. There was little consistency in model performance between sites and years, so no overall best model could be identified.

Twenty-one models submitted simulations driven by 18 years of meteorological observations for a grassland site at Valdai, Russia for PILPS2d [91,95]. The models as a group captured the broad features of snow accumulation and ablation, but differences in predictions of mid-winter melt led to systematic scatter between models.

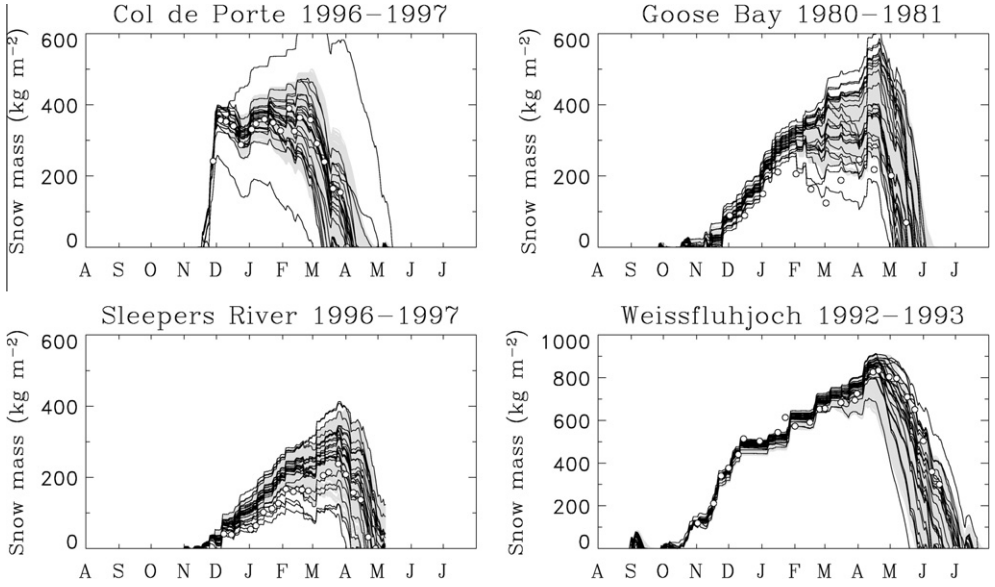

Fig. 1. Measurements of snow mass (circles) compared with simulations by the 23 models that participated in SnowMIP (black lines) and the 1701 model configurations described here (grey lines). Note that the driving data supplied for Sleepers River ended on 31 May 1997, at which time not all of the models had melted all of the snow.

Please cite this article in press as: Essery R et al. A comparison of 1701 snow models using observations from an alpine site. Adv Water Resour (2012), http://dx.doi.org/10.1016/j.advwatres.2012.07.013

Snow albedo, fractional snow cover and model structure had large and interacting influences on the absorption and partitioning of energy by snow. The best combination of parameterizations could not be discerned.

Twenty years of driving data were provided for 218 0.25° grid cells covering the Torne and Kalix river basins in northern Scandinavia and 21 models participated in PILPS2e [13,76]. The experiment was partly limited by the poor availability of reliable precipitation and radiation data, which is a common problem for high latitude studies. All of the models captured the broad dynamics of snow melt and runoff, but there were large differences between models, particularly during the spring melt period. Differences between predictions of annual runoff were primarily related to differences in predictions of winter snow sublimation, for which the models' formulations of aerodynamic resistances and stability corrections were important. Differences in how models represented retention of melt water in snow influenced the timing of peaks in runoff rather than their magnitude. The complexity of the participating models made the interpretation of results difficult, and differences in model complexity did not explain differences in results. Those models that took the opportunity offered to calibrate parameters using data from small catchments had lower errors in runoff simulations for the whole basin than those that did not.

Rhône-AGG [12] investigated the impact of spatial scale on simulations of water balance in the Rhône basin, for which about 10% of the annual precipitation is snow. Of the 15 land surface models participating, those that included explicit snow schemes gave the best simulations of snow depth in comparison with observations at 24 sites and had consistently larger snow depths than simpler composite schemes.

3. Model driving and evaluation data

Data from the Météo-France site at Col de Porte (45.3°N, 5.77°E, 1325 m a.s.l.) in the Chartreuse massif near Grenoble are used in this study. Snow lies for about 5 months each year (from December to April) and the maximum snow depth has reached 1.5 m in recent years (greater snow depths occurred in the 1960s). The main melting period begins in March or April, but air temperatures can rise above 0 °C and rain can fall in any month of the year. The snowpack is often wet and is typical of mid-elevation, mid-latitude mountain ranges. Col de Porte data have been used in SnowMIP and numerous other snow modelling studies (e.g. [10,15,16,36,97,100,105,110]). Four winters, beginning in 2005, are considered here; meteorological conditions are shown in Fig. 2. Compared with 2005–2006, the winter of 2006–2007 was warmer and less snowy, 2007–2008 was warmer and *more* snowy, and 2008–2009 was similar.

Energy balance models typically require inputs of incoming shortwave radiation $SW_{\downarrow}$ (W m^{-2}), incoming longwave radiation $LW_{\downarrow}$ (W m^{-2}), rainfall rate R_f (kg m^{-2} s^{-1}), snowfall rate S_f (kg m^{-2} s^{-1}), air temperature T_a (K), relative humidity RH (%), wind speed U_a (m s^{-1}) and atmospheric pressure P_a (Pa). All of these variables are measured at Col de Porte: air temperature, humidity and pressure are measured once an hour, precipitation amounts are cumulated and radiation fluxes and wind speed are averaged over each hour. Air temperature and humidity are measured at height $z_T = 2$ m above the snow surface and wind speed at $z_U = 10$ m. Relative humidity can be converted to specific humidity

$$Q_a = (RH/100)Q_{\mathrm{sat}}(T_a, P_a), \tag{1}$$

where Q_{sat} is the saturation specific humidity.

Data from many sites have been used for snow modelling, but the systems installed at Col de Porte provide data of unusually high quality and completeness [74]. Shortwave and longwave radiation sensors are mounted on a rotating arm which automatically passes through a cleaning and defrosting unit every hour, eliminating the need for continuous heating or ventilation. Heated gauges provide separate measurements of rainfall and snowfall , corrected for undercatch as a function of wind speed following Forland et al. [47]. Temperature and humidity sensors are mounted on a vertical rail and adjusted weekly to maintain their height relative to the snow surface.

Variables measured at Col de Porte which can be used for model evaluation include outgoing shortwave and longwave radiation, from which surface albedo and temperature can be calculated. Snow depth is measured both manually and automatically by ultrasonic ranging. Snow mass data used in previous model evaluations have mostly come from infrequent manual gravimetric measurements, but snow mass is also measured using a cosmic ray attenuation sensor [61,82] installed at Col de Porte by the Division Technique Générale of the EDF energy company. Calibration of this sensor against manual snow mass measurements on a yearly basis

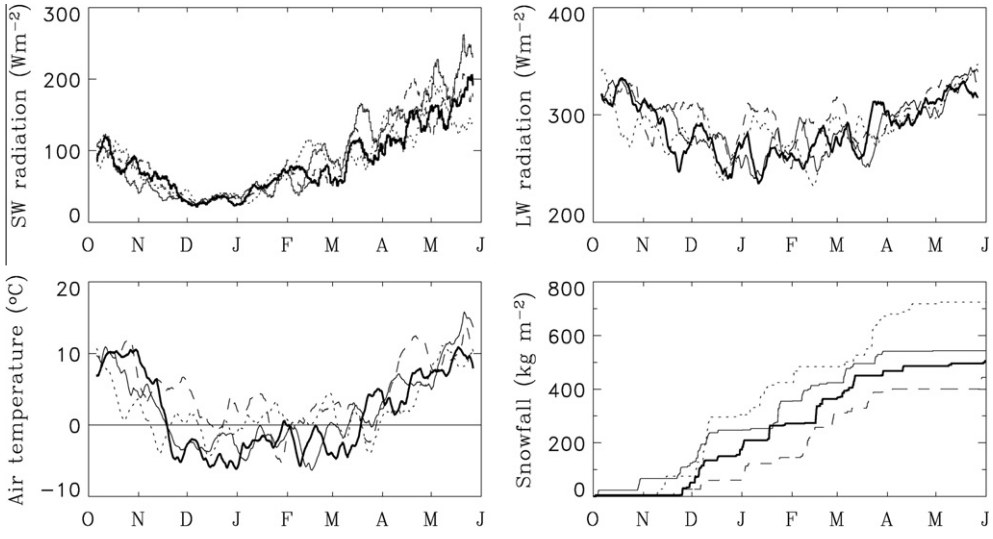

Fig. 2. Ten-day running means of incoming shortwave radiation, incoming longwave radiation and air temperature, and cumulative snowfall at Col de Porte in 2005–2006 (thick black lines), 2006–2007 (dashed lines), 2007–2008 (dotted lines) and 2008–2009 (thin black lines).

Please cite this article in press as: Essery R et al. A comparison of 1701 snow models using observations from an alpine site. Adv Water Resour (2012), http://dx.doi.org/10.1016/j.advwatres.2012.07.013

provides accurate interpolation of weekly manual measurements to the daily time scale. Automatic snow mass and depth measurements generally agree well with manual measurements and typically show snow densities approaching 400 kg m^{-3} towards the end of each winter at Col de Porte. Because the measurements are not all made at exactly the same point, however, inconsistencies can arise due to spatial variations in the snow cover, particularly for shallow snow conditions as in 2006–2007.

4. Model structure

Physical snow models are based on mass and energy conservation equations. Model developers have to make decisions about how to parameterize (or neglect) flux terms in these equations, how to parameterize the thermal, hydraulic, mechanical and radiative properties of snow that determine the fluxes, how to select values for parameters and how to solve the equations. JIM uses a range of previously published parameterizations in different combinations, with the same numerical solution method in all cases.

The mass per unit volume of snow can be divided into solid ice and liquid water contents γ_i and γ_w with separate conservation equations. Neglecting horizontal water flow and horizontal transport of snow by wind and avalanches (all of which can be represented by specialized models), these equations are

$$\frac{\partial \gamma_i}{\partial t} = \frac{\partial Q_i}{\partial z} - m \tag{2}$$

and

$$\frac{\partial \gamma_w}{\partial t} = \frac{\partial Q_w}{\partial z} + m, \tag{3}$$

where z is height above the ground, m is a volumetric rate of phase change (positive for melt and negative for refreezing) and Q_i and Q_w are vertical solid and liquid mass fluxes (positive downwards). Boundary conditions for Eqs. (2) and (3) are given by

$$Q_i = S_f - E_i, \qquad Q_w = R_f - E_w \tag{4}$$

at the snow surface and

$$Q_i = 0, \qquad Q_w = R_0 \tag{5}$$

at the base of the snowpack, where E_i is sublimation of ice, E_w is evaporation of liquid water and R_0 is drainage of liquid water. The snow density is $\rho_s = \gamma_i + \gamma_w$. Total ice mass, liquid water mass and melt rate per unit ground area for a snowpack of depth d_s are given by

$$I = \int_0^{d_s} \gamma_i(z)\, dz, \tag{6}$$

$$W = \int_0^{d_s} \gamma_w(z)\, dz \tag{7}$$

and

$$M = \int_0^{d_s} m(z)\, dz. \tag{8}$$

Snow water equivalent depth (SWE) is often quoted interchangeably with total mass per unit area, although strictly they are related by $I + W = \rho_w$SWE; assuming $\rho_w = 1000$ kg m^{-3} for the density of water gives 1 mm water equivalent $\equiv$ 1 kg m^{-2}.

Neglecting penetration of shortwave radiation and advection of heat by liquid water (both of which are included in some models), conservation of energy in a snowpack with vertical temperature profile $T_s(z,t)$ gives

$$c_s \frac{\partial T_s}{\partial t} = \frac{\partial G}{\partial z} - L_f m, \tag{9}$$

where $c_s = c_i\gamma_i + c_w\gamma_w$ is the volumetric heat capacity of the snow, G is vertical heat flux and L_f is the latent heat of fusion (constants that are not otherwise defined in equations are given in Table 2). JIM has separate prognostic variables for snow temperature and liquid water content, but this is not actually necessary; both can be diagnosed from a prognostic heat content $c_s(T_s - T_m) - L_f\gamma_w$ [68].

JIM follows those models that balance net radiation with sensible, latent and conducted heat fluxes for an infinitesimal surface skin layer at temperature T_{ss}, giving

$$(1-\alpha_s)SW_\downarrow + \epsilon(LW_\downarrow - \sigma T_{ss}^4) = H_s + L_sE_i + L_cE_w + L_fM_s + Q_p - G(d_s), \tag{10}$$

where α_s is the snow albedo, ϵ is the surface emissivity (invariably set to a constant close to or equal to 1 for snow), M_s is surface melt rate, Q_p is heat advected by precipitation (included in some models but neglected here) and H_s is the sensible heat flux from the snow to the atmosphere. When parameterizations for the fluxes are inserted on the right-hand side, this becomes a nonlinear equation for T_{ss} which can be solved by iteration or linearization; an algebraic solution of the linearized equation, following Best et al. [8], is used in JIM for computational efficiency. The net flux $G(d_s)$ at the snow surface provides an upper boundary condition for Eq. (9), and the heat flux at the base of the snowpack is calculated by coupling to a soil model adapted from JULES [8]. The melt rate is diagnosed by ensuring that the snow surface temperature does not exceed 0 °C.

Numerical solution of the coupled mass and energy conservation equations requires discretization in space and time, and Clark and Kavetski [19] have shown that the choice of numerical solution method has large influences on hydrological model predictions. Strong vertical temperature, density and liquid water content gradients can develop in snow, and many thin models layers have to be used if these gradients are to be explicitly represented by finite differences. Boone et al. [12] classified snow models as "composite" if they calculate a surface energy balance for a combined layer of snow and soil and "explicit" if they use one or more distinct layers to represent snow. Rather than having a fixed number of layers as soil models do, multi-layer snow models use increasing numbers of layers with increasing snow depth up to some maximum number. This number is arbitrary in SNOWPACK, 50 in Crocus, 5 in CLM, 3 in ISBA-ES, MATSIRO and SAST, 2 in SNOBAL and VIC and user specified in JULES. BASE, CLASS and HTESSEL are single-layer explicit models, and ISBA-FR, MOSES and SSiB are composite models. JIM uses a maximum of three layers, with a fixed surface layer depth of 0.1 m when the snow depth exceeds 0.2 m and a fixed second layer depth of 0.2 m when it exceeds 0.5 m. Eq. (10) is solved analytically to find the surface net heat flux and melt rate,

Table 2
Physical constants and quantities taken as constant in JIM.

Constant	Value	Description
c_i	2100 J K^{-1} kg^{-1}	Specific heat capacity of ice
c_a	1005 J K^{-1} kg^{-1}	Specific heat capacity of air
c_w	4180 J K^{-1} kg^{-1}	Specific heat capacity of water
g	9.81 m s^{-2}	Acceleration due to gravity
k	0.4	Von Kàrmàn constant
L_c	2.501×10^6 J kg^{-1}	Latent heat of condensation
L_f	0.334×10^6 J kg^{-1}	Latent heat of fusion
L_s	2.835×10^6 J kg^{-1}	Latent heat of sublimation
λ_a	0.025 W m^{-1} K^{-1}	Thermal conductivity of air
λ_i	2.24 W m^{-1} K^{-1}	Thermal conductivity of ice
R	287 J K^{-1} kg^{-1}	Gas constant for dry air
ρ_i	917 kg m^{-3}	Density of ice
ρ_w	1000 kg m^{-3}	Density of water
σ	5.67×10^{-8} W m^{-2} K^{-4}	Stefan–Boltzmann constant
T_m	273.15 K	Melting point

Please cite this article in press as: Essery R et al. A comparison of 1701 snow models using observations from an alpine site. Adv Water Resour (2012), http://dx.doi.org/10.1016/j.advwatres.2012.07.013

and Eq. (9) is then solved by the Crank–Nicolson method [25], initially assuming no phase changes within layers. If liquid content exceeds the capacity of a layer, water is then drained to the next lowest layer. Finally, liquid water in any layer with a temperature below 0 °C is frozen and the liquid water content, ice content and temperature of the layer are adjusted according to Eqs. (2), (3) and (9). A fixed timestep of 3600 s is used, which matches the period of the driving data.

To calculate fluxes in the mass and energy balance equations, models require parameterizations of processes determining the albedo, thermal conductivity, liquid water content and fractional coverage of snow on the ground, the density of fresh and compacted snow and exchanges of heat and moisture between snow and the atmosphere. Drawing on existing models for each process, JIM aims to provide a physically-based parameterization option, an empirical parameterization option and an option in which a process is represented by a constant or simply neglected. In some cases, such as for the parameterization of fresh snow density, there are only empirical parameterizations in common use; three options are then selected to represent a range of current models. Parameterizations are described in the following subsections, with examples of models using each option. Some models offer choices of parameterizations or have used different parameterizations at different times in their development, so particular models are sometimes mentioned more than once in a subsection. Different models may use the same parameterization for a particular process but choose different parameter values, so a literature source is given for every parameter set.

4.1. Snow compaction

The density of snow generally increases over time due to settling of grains as they metamorphosize into more rounded forms, compaction under the weight of overlying snow and refreezing of melt water. Models often parameterize the thermal conductivity and liquid water capacity of snow as functions of density (see Sections 4.6 and 4.7) and density is required for diagnosis of snow depth from mass. Snow mass is a model state variable, but snow depth is much more commonly measured, so modelled values of snow density are used with measurements of depth to initialize snow mass in forecasting models [14,33]. Physical, empirical and constant compaction options are available in JIM.

4.1.1. Option 0: physical snow compaction parameterization

CLM, COUP, HTESSEL, IAP94, ISBA-ES, SAST, SNTHERM, VIC and VISA all use a compaction parameterization following Anderson [3] in which there is rapid settling of fresh, low density snow followed by slower densification under load resisted by a compactive viscosity. The rate of change in the density ρ_s of a snow layer with temperature T_s and overlying mass M_s is given by

$$\frac{1}{\rho_s}\frac{d\rho_s}{dt} = \frac{M_s g}{\eta} + c_1 \exp[-c_2(T_m - T_s) - c_3 \max(0, \rho_s - \rho_0)], \quad (11)$$

Table 3
Parameter values for snow compaction parameterizations.

Option	Equations	Parameters	
0	(11) and (12)	Boone [11]	
		$c_1 = 2.8 \times 10^{-6}$ s^{-1}	$c_2 = 0.042$ K^{-1}
		$c_3 = 0.046$ m^3 kg^{-1}	$c_4 = 0.081$ K^{-1}
		$c_5 = 0.018$ m^3 kg^{-1}	$\rho_0 = 150$ kg m^{-3}
		$\eta_0 = 3.7 \times 10^7$ kg m^{-1} s^{-1}	
1	(14)	Verseghy [104]	
		$\rho_{max} = 300$ kg m^{-3}	$\tau_\rho = 3.6 \times 10^5$ s
2	Constant	Cox et al. [23]	$\rho_s = 250$ kg m^{-3}

where the viscosity is

$$\eta = \eta_0 \exp[c_4(T_m - T_s) + c_5\rho_s]. \quad (12)$$

Values for the seven parameters in Eqs. (11) and (12) given in Table 3 are taken from ISBA-ES. A slightly simplified form of Eq. (11) without the c_1 term for initial compaction is used by BASE, JULES and Lynch-Stieglitz [68]. Quite different values for η_0 are used by BASE (10^7 Pa s), CLM (8.8×10^6 Pa s), ISBA-ES (3.7×10^7 Pa s) and SNTHERM (3.6×10^6 Pa s), even though they all quote the same sources.

4.1.2. Option 1: empirical snow compaction parameterization

A hypothesis that snow density increases at a rate proportional to the difference between the current density and a maximum attainable density ρ_{max} can be expressed as a differential equation

$$\frac{d\rho_s}{dt} = \tau_\rho^{-1}(\rho_{max} - \rho_s), \quad (13)$$

where τ_ρ is an empirically determined compaction time scale. Integrating over a timestep of length δt then gives

$$\rho_s(t + \delta t) = \rho_{max} + [\rho_s(t) - \rho_{max}]\exp(-\delta t/\tau_\rho). \quad (14)$$

This difference equation is used for snow compaction in CLASS, HTESSEL and ISBA-FR. Values for the two parameters given in Table 3 were obtained by Verseghy [104] from earlier field measurements.

4.1.3. Option 2: constant snow density

Some models, including MAPS, MATSIRO, MOSES and SiB, neglect compaction and take fixed values for ρ_s. The value of 250 kg m^{-3} given in Table 3 is used by MOSES.

4.1.4. Comparison of compaction parameterizations

Coupled to a parameterization of fresh snow density (4.2) but isolated from the rest of the snow model, compaction parameterizations can be simply driven with measured snowfall and snow temperature inputs as long as there is no freezing of infiltrating water. Fig. 3 shows observations and simulations of snow depth and density for the cold period between December 2005 and February 2006. Option 0 gives the best simulation of density, and the constant density in option 2 can at best be a compromise between an overestimate for fresh snow and an underestimate for compacted snow. Deficiencies in option 1 for simulating snow densities at Col de Porte and other SnowMIP sites were identified by Bartlett et al. [7] and Dutra et al. [34]; as a result, a new parameterization was developed for version 3.1 of CLASS and the SNTHERM parameterization has now been adopted in HTESSEL.

4.2. Fresh snow density

The density of newly deposited snow depends on the size, shape and packing of the snow crystals, which depend on temperature and humidity during their formation and wind during deposition (Zwart et al., this volume), but there are no physical models of the deposition process in use. Crocus, HTESSEL and ISBA-ES use an empirical function of air temperature and wind speed for fresh snow density

$$\rho_f = \max[a_f + b_f(T_a - T_m) + c_f U_a^{1/2}, \rho_{min}] \quad (15)$$

based on measurements at Col de Porte, and CLM and Noah use a function of temperature alone

$$\rho_f = \rho_{min} + \max[d_f(T_a - T_m + e_f)^{3/2}, 0] \quad (16)$$

from Anderson [3]; parameter values are given in Table 4. Other empirical parameterizations are given by Hedstrom and Pomeroy

Please cite this article in press as: Essery R et al. A comparison of 1701 snow models using observations from an alpine site. Adv Water Resour (2012), http://dx.doi.org/10.1016/j.advwatres.2012.07.013

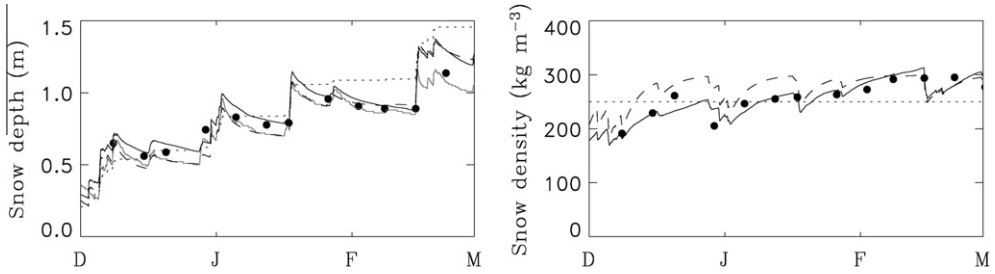

Fig. 3. Snow depth and density from manual measurements (circles) in 2005–2006 and simulations with compaction parameterization options 0 (solid lines), 1 (dashed lines) and 2 (dotted lines). The grey line shows snow depth measured by an ultrasonic gauge.

Table 4
Parameter values for fresh snow density parameterizations.

Option	Equations	Parameters	
0	(15)	Boone [11]	
		$a_f = 109$ kg m^{-3}	$b_f = 6$ kg m^{-3} K^{-1}
		$c_f = 26$ kg m$^{-7/2}$ s$^{1/2}$	$\rho_{min} = 50$ kg m^{-3}
1	(16)	Oleson et al. [80]	$d_f = 1.7$ K^{-1}
		$e_f = 15$ K	$\rho_{min} = 50$ kg m^{-3}
2	Constant	Douville et al. [32]	$\rho_f = 100$ kg m^{-3}

[56], Fassnacht and Soulis [43], Lehning et al. [63] and Roebber et al. [87]. Eqs. (15) and (16) are taken as options 0 and 1 for JIM, and option 2 is to use a fixed density for fresh snow as in BASE, BATS, CLASS, HTESSEL, ISBA-FR, JULES, SiB and SPONSOR. A density of 100 kg m^{-3} corresponds with the popular rule-of-thumb that 1 cm of snowfall contains 1 mm of water [87], but lower densities of 50 or 80 kg m^{-3} are also used in some models.

Fresh snow density can be estimated by dividing hourly measurements of snowfall by hourly changes in measured snow depth; results for the four years of hourly data used here, shown in Fig. 4(a), are highly scattered. Averaging the data into 2 °C temperature classes for wind speeds greater than or less than 2 m s^{-1} shows a clear increase in fresh snow density with increasing air temperature and some increase for greater wind speeds.

A variable snowfall density cannot be used if a fixed density is used for snow on the ground. In either the physical or empirical snow compaction options, however, the bulk density of a snow layer with initial density ρ_{s0} and mass M_s after addition of an amount $S_f\delta t$ of snowfall with density ρ_f is

$$\rho_s = \frac{M_s + S_f\delta t}{M_s/\rho_{s0} + S_f\delta t/\rho_f}. \quad (17)$$

As an example of the influence of snowfall on depth, Fig. 4(b) shows the increase in snow depth and compaction following a snowfall event on 18 January 2006. 49 mm water equivalent of snow fell over 18 h at temperatures around −1 °C and wind speeds up to 2.2 m s^{-1}. In this case, fresh snow density options 0 and 1 match the initial 30 cm increase in snow depth well but it is overestimated by option 2. Densification of the snow over a few days thereafter using the physical compaction option reduces the difference in snow depths given by the different fresh snow density parameterization options.

4.3. Snow albedo

The fraction of shortwave radiation reflected from snow is high and depends on the grain structure, contaminant concentration and depth of the snow. This has major impacts on the energy balance of snow-covered surfaces, the timing of snow melt and climate feedbacks involving changes in snow cover. Because reflection from snow also depends strongly on the wavelength and incidence angle of radiation, however, the hemispherically and spectrally averaged albedo is not an intrinsic property of a snow surface but also depends on the angular and spectral distribution of the incident radiation. Spectral models such as those of Wiscombe and Warren [108], Green et al. [50] and Kokhanovsky and Zege [62] can predict snow reflectance in great detail but are too computationally expensive for use in energy balance snow models. Some parameterizations instead calculate a single snow albedo and others calculate separate albedos for direct-beam and diffuse radiation in visible and near-infrared wavebands.

4.3.1. Option 0: physical snow albedo parameterization

Efficient parameterizations developed by Marshall and Warren [72] and Marks and Dozier [69] from the spectral snow albedo

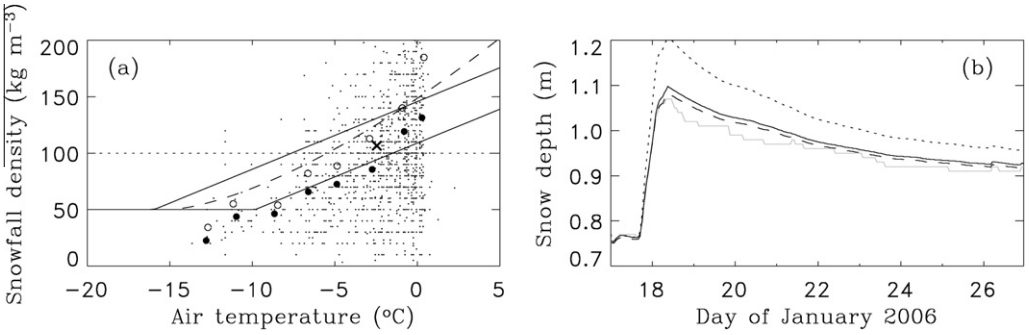

Fig. 4. (a) Fresh snow densities from hourly snowfall and depth change measurements (small dots), averaged into 2 °C temperature classes for wind speeds less than (solid circles) and greater than 2 m s^{-1} (open circles) and compared with parameterization option 0 for 0 and 2 m s^{-1} wind speeds (lower and upper solid lines), option 1 (dashed line) and option 2 (dotted line). The cross shows the average temperature and density for all recorded snowfall events. (b) Snow depth measured by the ultrasonic depth gauge (grey line) in January 2006 and simulated with the physical compaction option and fresh snow density parameterization options 0 (solid line), 1 (dashed line) and 2 (dotted line).

Please cite this article in press as: Essery R et al. A comparison of 1701 snow models using observations from an alpine site. Adv Water Resour (2012), http://dx.doi.org/10.1016/j.advwatres.2012.07.013

model of Wiscombe and Warren [108] have been adopted in MOSES and SNOBAL and implemented in the NCAR community climate model [71]. Flanner and Zender [45,46] have developed a new snow microphysics and albedo model that has now been adopted in CLM4 [81] and is likely to be widely used in the future, but another parameterization based on Wiscombe and Warren [108] with a longer history of use in snow models is taken as the most physical snow albedo option in JIM; it was introduced by Dickinson et al. [29] for use in BATS and has also been used in CLM3, IAP94, Noah-MP and the model of Jin et al. [59]. There are 10 parameters, values for which are listed in Table 5. Albedos for diffuse radiation in the visible and near-infrared bands are

$$\alpha_{\mathrm{dif,\,vis}} = (1 - C_{\mathrm{vis}} F_{\mathrm{age}})\alpha_{\mathrm{vis},0} \tag{18}$$

and

$$\alpha_{\mathrm{dif,\,nir}} = (1 - C_{\mathrm{nir}} F_{\mathrm{age}})\alpha_{\mathrm{nir},0} \tag{19}$$

with snow age factor

$$F_{\mathrm{age}} = \frac{\tau_s}{1 + \tau_s}. \tag{20}$$

The non-dimensional snow age τ_s increases with time and is decreased by snowfall according to

$$\tau_s(t + \delta t) = [\tau_s(t) + (r_1 + r_2 + r_3)\tau_0^{-1}\delta t]\left(1 - \frac{S_f \delta t}{S_0}\right) \tag{21}$$

with

$$r_1 = \exp\left[T_\alpha\left(\frac{1}{T_m} - \frac{1}{T_s}\right)\right] \tag{22}$$

representing the effect of grain growth due to vapour diffusion, $r_2 = r_1^{10}$ representing more rapid growth close to the melting point and constant r_3 representing the effect of contaminants in the snow. The visible and near-infrared albedos for direct-beam radiation are

$$\alpha_{\mathrm{dir,\,vis}} = \alpha_{\mathrm{dif,\,vis}} + a_\mu f(\mu)(1 - \alpha_{\mathrm{dif,\,vis}}) \tag{23}$$

and

$$\alpha_{\mathrm{dir,\,nir}} = \alpha_{\mathrm{dif,\,nir}} + a_\mu f(\mu)(1 - \alpha_{\mathrm{dif,\,nir}}), \tag{24}$$

where

$$f(\mu) = \max\left[\frac{1 - 2\mu}{1 + b_\mu \mu}, 0\right] \tag{25}$$

for solar zenith cosine μ, giving increased albedos for zenith angles greater than 60°.

4.3.2. Option 1: empirical snow albedo parameterization

Similarly to the empirical snow compaction parameterization described in Section 4.1.2, empirical snow albedo decay parameterizations can be formulated as differential equations and integrated to give the change in albedo over a timestep. The empirical option selected for JIM is taken from ISBA and HTESSEL, in which albedo has a linear decay with time

$$\alpha_s(t + \delta t) = \alpha_s(t) - \tau_\alpha^{-1}\delta t \tag{26}$$

for cold snow and an exponential decay

$$\alpha_s(t + \delta t) = [\alpha_s(t) - \alpha_{\mathrm{min}}]\exp(-\tau_m^{-1}\delta t) + \alpha_{\mathrm{min}} \tag{27}$$

for melting snow. Snowfall refreshes the snow albedo by an amount

$$\delta\alpha_s = (\alpha_{\mathrm{max}} - \alpha_s)\frac{S_f \delta t}{S_0} \tag{28}$$

up to the maximum fresh snow albedo α_{max}. The five parameters for this option are given in Table 5. CLASS and Noah-MP use the same approach, except that Eq. (27) is used for both cold and melting snow with different values of α_{min} and different maximum albedos are used for visible and near-infrared wavelengths.

4.3.3. Option 2: snow temperature albedo parameterization

Although the snow albedo parameterizations described in Sections 4.3.1 and 4.3.2 are simple to code, they do require prognostic snow albedo or age variables to be held in memory. Although it is no longer a limitation, it used to be common for global climate models to avoid this computational expense by simply diagnosing snow albedo as a function of surface temperature, and such models are still in common use; examples include the snow albedo parameterizations in the ECHAM3 [28] and HadCM3 [23] climate models and SiB in the CSU and COLA climate models [86,109]. Typically, the albedo is made to decrease linearly from a maximum value below a critical temperature to a minimum at the melting point, according to

$$\alpha_s = \alpha_{\mathrm{max}} + (\alpha_{\mathrm{min}} - \alpha_{\mathrm{max}})\max\left(\frac{T_s - T_c}{T_m - T_c}, 0\right). \tag{29}$$

Parameter values used here are given in Table 5.

4.3.4. Comparison of albedo parameterizations

All of the snow albedo parameterization options require snowfall and snow temperature as inputs. In the full model, snowfall is provided by observations and temperature is determined by energy balance, but the albedo parameterizations can be decoupled from their role in the surface energy balance by using observed surface temperature as an input; this approach was used in evaluations of snow albedo parameterizations from weather forecasting and climate models by Pedersen and Winther [83] and Wang and Zeng [107]. The direct and diffuse fluxes in spectral bands required by parameterizations that calculate separate albedos are simulated by the radiative transfer schemes in atmospheric models but are seldom measured and were not provided in any of the major intercomparison projects discussed above. Global all-band shortwave radiation measurements at Col de Porte are regularly partitioned into direct and diffuse spectral components for driving Crocus, and the same components are used here for driving snow albedo parameterization option 0.

Observations and simulations of albedo in 2005–2006 are shown in Fig. 5. The effective albedo for thin or partial snow cover is taken to be

$$\alpha = f_s\alpha_s + (1 - f_s)\alpha_0, \tag{30}$$

where α_0 is the snow-free albedo and the fraction f_s is given by Eq. (51) in Section 4.5. All of the albedo parameterization options capture the rapid transition from a low snow-free albedo to a high snow-covered albedo in November and back again in April, with a general decrease in albedo over the winter interrupted by snowfall events. Option 2 gives some spurious decreases in albedo during short warm periods.

Table 5
Parameter values for snow albedo parameterizations.

Option	Equations	Parameters		
0	(18)–(25)	Oleson et al. [80]		
		$\alpha_{\mathrm{vis},0} = 0.95$	$\alpha_{\mathrm{nir},0} = 0.65$	$a_\mu = 0.4$
		$b_\mu = 2$	$C_{\mathrm{nir}} = 0.5$	$C_{\mathrm{vis}} = 0.2$
		$r_3 = 0.3$	$S_0 = 10\ \mathrm{kg\ m^{-2}}$	$T_\alpha = 5000\ \mathrm{K}$
		$\tau_0 = 10^6\ \mathrm{s}$		
1	(26)–(28)	Douville et al. [32]		
		$\alpha_{\mathrm{max}} = 0.85$	$\alpha_{\mathrm{min}} = 0.5$	$S_0 = 10\ \mathrm{kg\ m^{-2}}$
		$\tau_\alpha = 10^7\ \mathrm{s}$	$\tau_m = 3.6 \times 10^5\ \mathrm{s}$	
2	(29)	Cox et al. [23]		
		$\alpha_{\mathrm{max}} = 0.8$	$\alpha_{\mathrm{min}} = 0.62$	$T_c = T_m - 2\ \mathrm{K}$

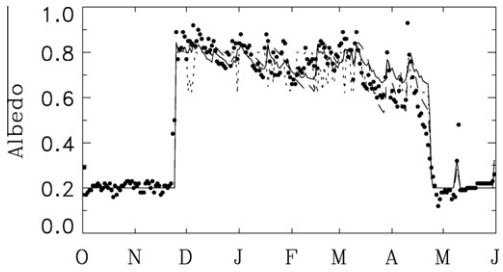

Fig. 5. Albedo measured in 2005–2006 (circles) and simulated with albedo parameterization options 0 (solid line), 1 (dashed line) and 2 (dotted line).

4.4. Surface heat and moisture fluxes

First-order closure is widely used to parameterize turbulent exchanges of heat and moisture between the atmosphere and the surface. Bulk aerodynamic formulae give sensible heat flux

$$H = \rho_a c_a C_H U_a (T_{ss} - T_a) \tag{31}$$

and moisture flux

$$E = \rho_a C_H U_a [Q_{\mathrm{sat}}(T_{ss}, P_a) - Q_a], \tag{32}$$

where $\rho_a = P_a/(RT_a)$ is the air density and C_H is an exchange coefficient, assumed to be the same for heat and moisture transport. Similarly, the flux of momentum from the atmosphere to the surface is parameterized as

$$\tau = -\rho_a C_D U_a^2 = -\rho_a u_*^2 \tag{33}$$

for drag coefficient C_D; this defines the friction velocity u_*.

Drag and exchange coefficients depend on atmospheric stratification, a surface roughness length for momentum (z_0) and a scalar surface roughness length (z_{0h}) for heat and moisture exchanges. Values of z_0 and z_{0h} are flow-dependent [5], but the common model assumption of constant values is used here. The same surface roughness values, given in Table 6, are used for all three surface flux options in JIM.

4.4.1. Option 0: Obukhov length parameterization

Atmospheric stratification can be characterized by the Obukhov length

$$L = -\frac{\rho_a c_a u_*^3 T_a}{kgH} \tag{34}$$

(strictly, the temperature here is the virtual potential temperature, not the air temperature). Monin–Obukhov similarity theory then gives the drag and exchange coefficients as

$$C_D = k^2 \left[\ln\left(\frac{z_U}{z_0}\right) - \psi_m\left(\frac{z_U}{L}\right) + \psi_m\left(\frac{z_0}{L}\right) \right]^{-2} \tag{35}$$

and

$$C_H = k C_D^{1/2} \left[\ln\left(\frac{z_T}{z_{0h}}\right) - \psi_h\left(\frac{z_T}{L}\right) + \psi_h\left(\frac{z_{0h}}{L}\right) \right]^{-1}. \tag{36}$$

Table 6
Parameter values for surface flux parameterizations.

Option	Equations	Parameters		
0	(40) and (41)	Zeng et al. [114]		
		$a = 16$	$b = 5$	$\mathrm{Ri}_{cr} = 1$
1	(49) and (50)	Louis [67]	$c = 5$	
2	(48)	Martin and Lejeune [73]		
All		$z_0 = 0.01$ m	$z_0/z_{0h} = 0.1$	

The stability functions ψ_m and ψ_h are integrals

$$\psi_{m,h} = \int_0^{z/L} \frac{1 - \phi_{m,h}(\zeta)}{\zeta} d\zeta \tag{37}$$

over the dimensionless ratio $\zeta = z/L$, where the gradient functions are

$$\phi_m = \frac{kz}{u_*}\frac{dU_a}{dz} \tag{38}$$

and

$$\phi_h = -kzu_*\frac{\rho_a c_a}{H}\frac{dT_a}{dz}. \tag{39}$$

Many functional forms for ϕ_m and ϕ_h are given in the literature; the review by Andreas [5] discusses which are most appropriate for use over snow surfaces. The functions chosen here are

$$\phi_m(\zeta) = \begin{cases} (1 - a\zeta)^{-1/4} & \zeta < 0 \\ 1 + b\zeta & 0 \leqslant \zeta \leqslant 1 \\ b + \zeta & \zeta > 1 \end{cases} \tag{40}$$

and

$$\phi_h(\zeta) = \begin{cases} (1 - a\zeta)^{-1/2} & \zeta < 0 \\ 1 + b\zeta & 0 \leqslant \zeta \leqslant 1 \\ b + \zeta & \zeta > 1 \end{cases} \tag{41}$$

with parameter values given in Table 6; these are taken from Zeng et al. [114] and are used in CLM. Obukhov length parameterizations are also used in COUP, HTESSEL, JULES, Noah-MP, SNOBAL, SWAP, VIC and VISA.

Integrating ϕ_m and ϕ_h from Eqs. (40) and (41) gives

$$\psi_m(\zeta) = 2\ln\left(\frac{1+x}{2}\right) + \ln\left(\frac{1+x^2}{2}\right) - 2\tan^{-1}x + \frac{\pi}{2} \tag{42}$$

and

$$\psi_h(\zeta) = 2\ln\left(\frac{1+x^2}{2}\right) \tag{43}$$

with $x = (1 - a\zeta)^{1/4}$ for $\zeta < 0$,

$$\psi_m(\zeta) = \psi_h(\zeta) = -b\zeta \tag{44}$$

for $0 \leqslant \zeta \leqslant 1$, and

$$\psi_m(\zeta) = \psi_h(\zeta) = (1 - b)(1 + \ln\zeta) - \zeta \tag{45}$$

for $\zeta > 1$.

Another measure of stratification, the gradient Richardson number, is related to the Obukhov length by

$$\mathrm{Ri} = \frac{\zeta\phi_h(\zeta)}{\phi_m^2(\zeta)}. \tag{46}$$

If Ri approaches a critical value Ri_{cr} as $\zeta \to \infty$, the surface decouples from the atmosphere ($C_H = 0$) for Richardson numbers exceeding Ri_{cr} and radiative cooling can lead to unrealistically low surface temperatures [27]. The choices for ϕ_m and ϕ_h in Eqs. (40) and (41) give $\mathrm{Ri}_{cr} = 1$, and Anderson [3] used stability functions with $\mathrm{Ri}_{cr} = 0.2$ which were found to give poor simulations when used in SNTHERM [60] and Crocus [73].

4.4.2. Option 1: Richardson number parameterization

The use of Monin–Obukhov similarity theory to calculate surface fluxes in early numerical weather prediction and climate models presented two problems addressed by Louis [67]: the computational cost of the iterative solution required for unstable conditions and surface decoupling in stable conditions. Instead,

the exchange coefficient can be parameterized as $C_H = F_H(\mathrm{Ri_B})C_{HN}$ where F_H is a function of the bulk Richardson number

$$\mathrm{Ri_B} = \frac{gz_U(T_a - T_{ss})}{T_a U_a^2} \tag{47}$$

and

$$C_{HN} = k^2\left[\ln\left(\frac{z_U}{z_0}\right)\right]^{-1}\left[\ln\left(\frac{z_T}{z_{0h}}\right)\right]^{-1} \tag{48}$$

is the exchange coefficient for neutral stratification ($\mathrm{Ri_B} = 0$). Louis [67] approximated the iterative solution by an analytical function

$$F_H(\mathrm{Ri_B}) = 1 - \frac{3c\mathrm{Ri_B}}{1 + 3c^2 C_{HN}(-\mathrm{Ri_B} z_U/z_0)^{1/2}} \tag{49}$$

for the unstable case ($\mathrm{Ri_B} < 0$) and chose a function

$$F_H(\mathrm{Ri_B}) = \left[1 + \frac{2c\mathrm{Ri_B}}{(1 + \mathrm{Ri_B})^{1/2}}\right]^{-1} \tag{50}$$

with no critical cutoff for the stable case ($\mathrm{Ri_B} > 0$); a value for the single parameter c in Eqs. (49) and (50) is given in Table 6. Richardson number parameterizations with differing stability functions are used by BASE, BATS, CLASS, Crocus, IAP94, ISBA, MOSES and SNTHERM.

4.4.3. Option 2: constant exchange coefficient

Although SNOWPACK and Crocus are amongst the most sophisticated models in their representations of snow structure, they have options to use simple representations of turbulent fluxes in which stratification is neglected and constant values are taken for the exchange coefficient. Martin and Lejeune [73] obtained an average value of $C_H = 0.0034$ for wind speeds higher than 1 m s^{-1} by adjusting the exchange coefficient in Crocus to match simulated surface temperatures with nighttime observations at Col de Porte. This corresponds with a value of $z_0 = 0.015$ m in Eq. (48); the roughness lengths in Table 6 give a similar value of $C_H = 0.003$.

4.4.4. Comparison of surface flux parameterizations

Turbulent fluxes can be measured by eddy covariance or profile methods, and gradient functions can be fitted to data from simultaneous measurements by both methods. Such measurements are not regularly made at Col de Porte but would likely give highly site-specific results due to the complexity of the surrounding topography and forest cover. First-order closure is unable to represent the non-local scaling of turbulence over complex landscapes [57] and requires the use of effective parameter values; the calibrated roughness length for Col de Porte is an order of magnitude larger than textbook values given by, for example, Oke [79].

Fig. 6(a) shows C_H calculated by options 0–2 as functions of $\mathrm{Ri_B}$. Compared with option 0, the exchange coefficients for strongly stable conditions are higher in option 1 and much higher in option 2. A histogram of bulk Richardson number values calculated with observed surface temperature, air temperature and wind speed is shown in Fig. 6(b). The distribution is strongly peaked near 0 but has long tails, and $\mathrm{Ri_B}$ exceeded 1 for half of the hours between 1 October 2005 and 31 May 2006; option 0 will cut off the turbulent fluxes to the surface in these cases.

4.5. Snow cover fraction

4.5.1. Snow cover depletion curves

Redistribution of snow by wind, interception of snow by vegetation, different melt rates for snow on slopes of different aspects or under vegetation of different densities, topographic influences on the amount and phase of precipitation and the tracks of storms lead to variations in snow depths and heterogeneities in snow cover on centimetre to continental scales. Many spatial models that attempt to predict explicit snow distributions exist (e.g. [37,64,65,75], Winstral et al. this volume), but single-column models as discussed here have to represent unresolved heterogeneities in snow cover using functions of snow depth or mass and surface characteristics such as roughness length, vegetation height and variance of subgrid orography. This is crucial for large-scale models with grid scales that can encompass large variations in snow cover [77,88], but models often allow for partial snow cover even when run at point scales as here; the footprints of radiative and turbulent flux sensors used to obtain evaluation data can cover areas of snow, vegetation protruding above snow and snow-free ground.

The fractions of areas covered with snow during melt can be related to probability distributions of pre-melt snow mass [21,31], but models generally use snow cover depletion curves that relate fractional cover to average snow depth or mass. Functional forms in common use are reviewed by Essery and Pomeroy [39] and Liston [66]; all are empirical or conceptual, so the three options used here are selected to represent a typical range.

For average snow depth d_s, the snow cover fraction in BASE, BATS, CLM, IAP94 and JULES is given by

$$f_s = \frac{d_s}{d_s + d_0} \tag{51}$$

with differing parameters; CLM has $d_0 = 10z_{0g}$ for soil roughness length $z_{0g} = 0.01$ m. The same function, with snow mass in place of depth, is used by ECHAM and ISBA. Yang et al. [111] found that using the function

$$f_s = \tanh(d_s/d_0) \tag{52}$$

in BATS gave better agreement with albedo measurements, and Roesch [89] adopted the same form for flat, non-forested regions in ECHAM4. CLASS, HTESSEL and SiB use the linear function

$$f_s = \min(d_s/d_0, 1) \tag{53}$$

In JIM, Eq. (51) is used as option 0, Eq. (52) as option 1 and Eq. (53) as option 2. The single parameter d_0 is set to 0.1 m in all three

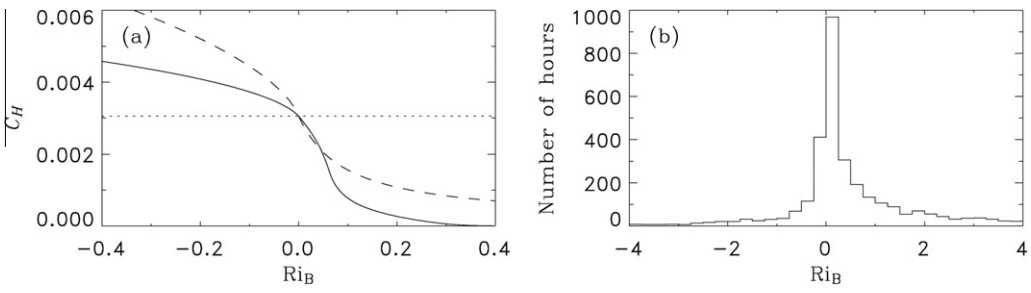

Fig. 6. (a) Exchange coefficients as functions of bulk Richardson number for surface flux parameterization options 0 (solid line), 1 (dashed line) and 2 (dotted line). (b) Histogram of bulk Richardson number values calculated from hourly air temperature, surface temperature and wind speed measurements in 2005–2006.

Please cite this article in press as: Essery R et al. A comparison of 1701 snow models using observations from an alpine site. Adv Water Resour (2012), http://dx.doi.org/10.1016/j.advwatres.2012.07.013

options. As can be seen from Fig. 7, a much greater depth of snow is required for complete cover with option 0 than options 1 or 2.

Models differ in how they use the snow cover fraction. It may be used to calculate effective parameters such as albedo and roughness length in a single energy balance calculation for combined snow and snow-free surfaces; this is known to lead to unrealistically early snowmelt in some situations [40,66]. Instead, JIM calculates area-average fluxes after separate energy balance calculations for the snow-covered and snow-free fractions of the surface.

4.5.2. Comparison of snow cover fraction parameterizations

Snow cover depletion curves can be fitted to data from repeated surveys measuring the depth of snow and the number of snow-free survey points during melt or can be predicted from measurements of pre-melt variability [21]. Such measurements are not regularly made at Col de Porte, so the snow cover fraction parameterizations are compared with albedo measurements instead. Inverting Eq. (30) gives

$$f_s = \frac{\alpha - \alpha_0}{\alpha_s - \alpha_0}, \tag{54}$$

which can be used to estimate f_s from albedo measurements if the albedos of the snow-covered and snow-free surfaces are known. Fig. 7 shows results obtained using $\alpha_0 = 0.2$ and assuming that $\alpha_s = 0.65$ for aged snow, compared with the three parameterization options. Option 0 gives the best fit, but the results depend strongly on the assumed value for α_s.

4.6. Snow hydrology

Gravitational drainage of liquid water from highly permeable snow at 0 °C is rapid and often involves preferential flow paths [2], but capillary tension retains an irreducible water content and can impede flow between snow layers of differing texture [58]. In addition to the partial water density γ_w, the liquid water content of snow can be expressed as a volumetric water content $\theta_w = \rho_w^{-1}\gamma_w$ or a water saturation $S_w = \phi^{-1}\theta_w$, where

$$\phi = 1 - \frac{\gamma_i}{\rho_i} \tag{55}$$

is the snow porosity. In terms of water saturation, the conservation equation for liquid water is

$$\frac{\partial U}{\partial z} + \phi\frac{\partial S_w}{\partial t} = \frac{m}{\rho_w} \tag{56}$$

with evaporation and rainfall boundary conditions. SNTHERM follows Colbeck [22] in neglecting capillary forces compared with gravity to take the vertical water velocity as

$$U = \frac{\rho_w g k_{\mathrm{sat}}}{\mu_w}\left(\frac{S_w - S_{wi}}{1 - S_{wi}}\right)^3, \tag{57}$$

where μ_w is the viscosity of water, k_{sat} is a saturated permeability parameterized as a function of snow density and grain size, and S_{wi} is the irreducible water saturation, described by Albert and Krajeski [1] as "one of the least well-understood parameters in snow physics". Explicit numerical solutions of Eq. (56) are unstable if water fluxes are large enough to saturate an initially dry snow layer within one timestep; SNTHERM uses an adaptive timestep to avoid this and Albert and Krajeski [1] presented an analytical solution. COUP and IAP94 adopted the SNTHERM flow parameterization, but other models almost invariably drain liquid water in excess of S_{wi} immediately, if they represent snow hydrology at all.

Parameterizing liquid flow velocities in snow greatly complicates a model and only makes a significant difference in runoff for deep snow or short timescales. JIM therefore uses two options in which liquid water drains immediately when it exceeds a holding capacity. Option 0 is used in ISBA-ES, HTESSEL, SAST and VISA, which follow Anderson [3] in setting a maximum liquid water mass fraction

$$\frac{\gamma_{w,\max}}{\rho_s} = r_{\min} + (r_{\max} - r_{\min})\max\left(1 - \frac{\rho_s}{\rho_r}, 0\right) \tag{58}$$

with parameter values given in Table 7. Option 1 has a fixed irreducible water saturation, giving

$$\gamma_{w,\max} = \rho_w \phi S_{wi}. \tag{59}$$

This is used with $S_{wi} = 0.033$ in CLM and 0.05 in Crocus; JIM uses the CLM value. As shown in Fig. 8, option 1 gives higher liquid capacities than option 0 for snow densities less than 500 kg m^{-3}. Other models impose a maximum volumetric water content (0.03 in Noah-MP and 0.08 in SNOWPACK) that is independent of density.

Many models, including BASE, BATS the original version of HTESSEL, ISBA-FR, MOSES and SSiB, neglect storage of liquid water in snow; surface melt water and rainfall are instantly translated to runoff at the base of the snowpack. This is used as option 2 in JIM and involves no parameters.

Liquid water is allowed to freeze and release latent heat if it drains into a snow layer with temperature below 0 °C in JIM configurations that can retain liquid water. Because this gives a strong

Table 7
Parameter values for snow hydrology parameterizations.

Option	Equations	Parameters		
0	(58)	Boone and Etchevers [10]		
		$r_{\min} = 0.03$	$r_{\max} = 0.1$	$\rho_r = 200$ kg m^{-3}
1	(59)	Oleson et al. [80]		$S_{wi} = 0.033$
2		None		

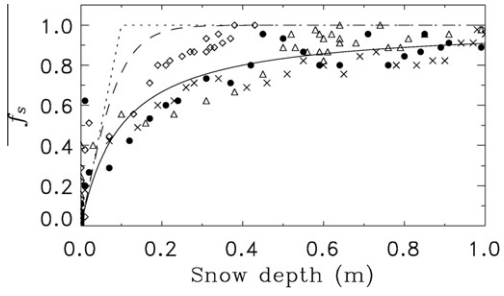

Fig. 7. Snow cover fraction parameterization options 0 (solid line), 1 (dashed line) and 2 (dotted line) compared with fractions inferred from albedo measurements in March and April of 2006 (circles), 2007 (diamonds), 2008 (triangles) and 2009 (crosses).

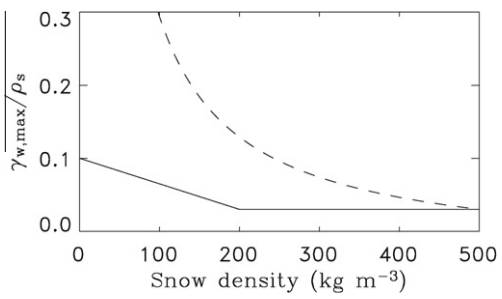

Fig. 8. Liquid water holding capacity of snow, expressed as a mass fraction, from snow hydrology parameterization options 0 (solid line) and 1 (dashed line).

Please cite this article in press as: Essery R et al. A comparison of 1701 snow models using observations from an alpine site. Adv Water Resour (2012), http://dx.doi.org/10.1016/j.advwatres.2012.07.013

coupling between the mass and energy balances, evaluations of the impacts of using different snow hydrology options are deferred until results are presented from the full model in Section 5.

4.7. Thermal conductivity of snow

Heat flux in snow with a vertical temperature gradient is given by

$$G = \lambda_s \frac{dT_s}{dz}, \tag{60}$$

where λ_s is an effective thermal conductivity for heat transfer processes including conduction through ice and vapour transport in the pore space. SNOWPACK links thermal conductivity to microstructural properties of snow, but other models almost invariably parameterize conductivity as a quadratic or power function of snow density; Slater et al. [95] listed the parameterizations used by all of the models that participated in PILPS2e. The three conductivity parameterization options in JIM are

$$\lambda_s = \lambda_a + (a_\lambda \rho_s + b_\lambda \rho_s^2)(\lambda_i - \lambda_a) \tag{61}$$

used in IAP94, SAST, SNTHERM and CLM,

$$\lambda_s = c_\lambda \left(\frac{\rho_s}{\rho_w}\right)^{n_\lambda} \tag{62}$$

from Yen [113] used in Crocus, HTESSEL, ISBA and JULES, and a fixed conductivity as used in MAPS and MOSES. Fig. 9 shows the three parameterization options with parameter values given in Table 8. Option 0 gives consistently higher conductivities than option 1; option 2 gives the highest conductivities for low density snow and the lowest conductivities for high density snow.

Measurements of thermal conductivity and regression equations relating them to snow density have been reviewed by Sturm et al. [98] and show a great deal of scatter, partly due to differences in snow structure and partly due to uncertainties in measurement methods [17]. Results from 3D modelling of conduction through ice and interstitial air in snow by Calonne et al. [17] closely follow the regression equation proposed by Yen [113].

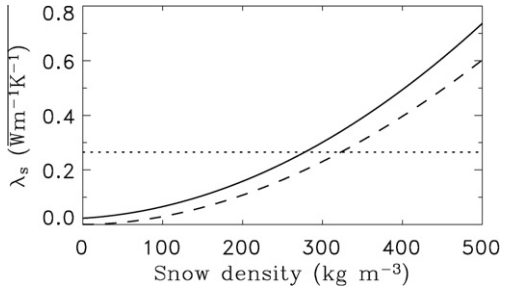

Fig. 9. Snow thermal conductivity parameterization options 0 (solid line), 1 (dashed line) and 2 (dotted line).

Table 8
Parameter values for thermal conductivity parameterizations.

Option	Equations	Parameters	
0	(61)	Oleson et al. [80]	
		$a_\lambda = 7.75 \times 10^{-5}$ m^3 kg^{-1}	$b_\lambda = 1.105 \times 10^{-6}$ m^6 kg^{-2}
1	(62)	Douville et al. [32]	
		$c_\lambda = 2.22$ W m^{-1} k^{-1}	$n_\lambda = 1.88$
2	Constant	Cox et al. [23]	$\lambda_s = 0.265$ W m^{-1} k^{-1}

4.8. Model classification

Each configuration of JIM is identified by a base-3 number

$$m = n_c n_s n_a n_e n_f n_h n_t \tag{63}$$

made up of the option numbers 0, 1 or 2 for compaction (n_c), fresh snow density (n_s), albedo (n_a), turbulent exchange (n_e), snow cover fraction (n_f), snow hydrology (n_h) and thermal conductivity (n_t) parameterizations. Rather than $3^7 = 2187$, there are $2 \times 3^6 + 3^5 = 1701$ possible model configurations because the variable snowfall density options are not used if snow compaction is neglected ($n_c = 2$). As a rough measure of complexity, the configurations have between 9 and 32 parameters. Although it does not give a unique specification, existing snow models can be classified by the same system. For example, MOSES as described by Cox et al. [23] is a composite 2*21122 model, CLASS as described by Verseghy [104] is a single-layer 1211200 model, CLM as described by Oleson et al. [80] is a multi-layer 0100010 model and Dutra et al. [34] upgraded HTESSEL from a composite 1210221 model to a single-layer 0010201 model.

5. Model spread

Before comparing simulations with observations, the spread in model predictions is discussed. Model spread has already been shown for snow mass simulations at the SnowMIP sites in Fig. 1, which includes results from the SnowMIP models and JIM. Excluding outliers due to models modifying the precipitation driving data, the ensemble of JIM simulations spans the range of the SnowMIP models well at all four sites.

JIM simulations of snow mass, snow depth, daily effective albedo and daily average surface temperature for the four recent winters at Col de Porte are shown in Figs. 10–13, and ensemble mean snow mass and spread are shown in Fig. 14. Mid-winter ensemble spread in snow mass is larger for the warm winters of 2006–2007 and 2007–2008 than the colder winters of 2005–2006 and 2008–2009, but the simulations have large spreads during spring melt in all years. The spread increases monotonically to a maximum in April each year, by which time some configurations are snow-free and others still have snow masses close to their maxima. Thereafter, the spread decreases rapidly as the remaining configurations melt the snow. Spread in snow depth is particularly large for the warm and snowy winter of 2007–2008. Spreads in albedo and surface temperature are largest at times when some model configurations have melted all of the snow and others have not.

The contributions of individual parameterizations to the ensemble spread can be measured by calculating differences between group means for simulations using each parameterization option and the full ensemble mean. Differences between snow mass simulations by configurations with different options for snow compaction, fresh snow density or thermal conductivity parameterizations turn out to be small, but choices for albedo, surface flux, snow cover fraction and snow hydrology parameterizations have larger impacts; these are shown for 2005–2006 in Fig. 15, and ensemble simulations for other winters give qualitatively similar behaviours. For albedo parameterization, option 0 gives the latest melt on average (shown by a positive difference from the ensemble mean snow mass) and option 2 the earliest. The two options which suppress turbulent fluxes in stable conditions give similar results, but the option of using a constant exchange coefficient gives earlier melt due to increased sensible heat flux to the snow in spring. Option 0 for snow cover fraction delays melt by reducing the surface area for transfer of heat from the atmosphere and absorption of radiation for a given volume of snow. The representation of snow hydrology has the biggest influence of any of the parameterizations;

Please cite this article in press as: Essery R et al. A comparison of 1701 snow models using observations from an alpine site. Adv Water Resour (2012), http://dx.doi.org/10.1016/j.advwatres.2012.07.013

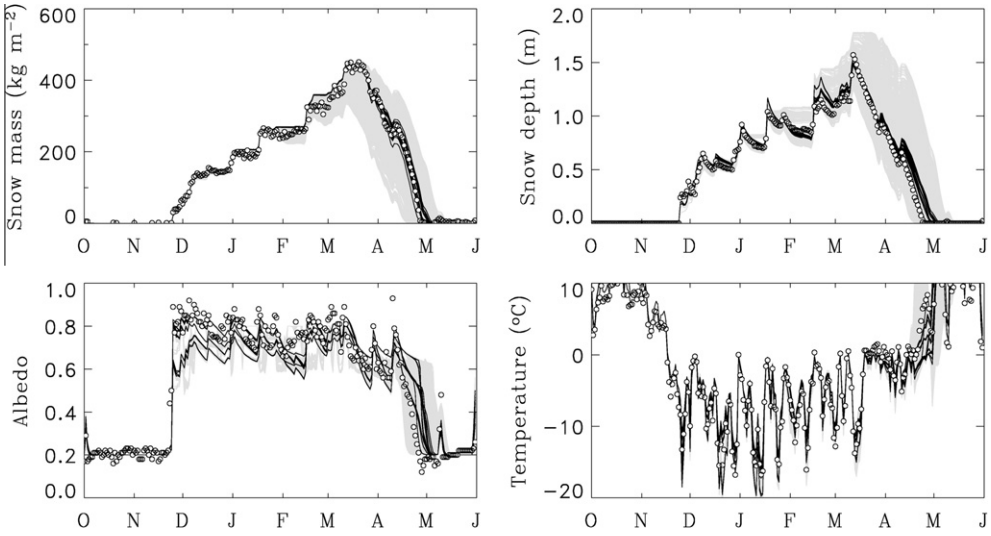

Fig. 10. Ensemble simulations (grey lines) and observations (circles) of snow mass, snow depth, daily effective albedo and daily average surface temperature at Col de Porte in 2005–2006. Black lines show simulations by configurations giving the 30 lowest values for a cost function of errors in all variables over all winters.

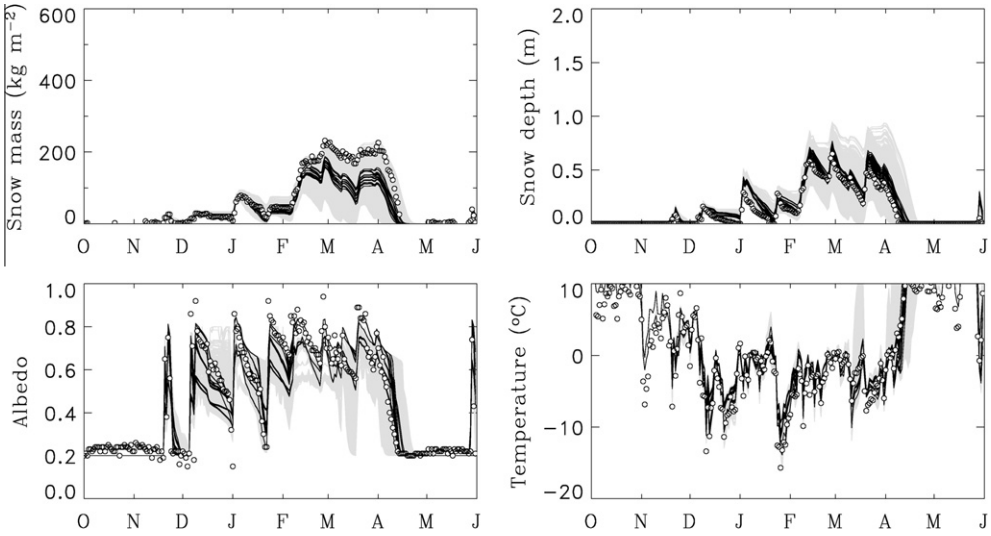

Fig. 11. As Fig. 10, but for 2006–2007.

configurations which use the highest liquid water capacity retain much higher snow masses than those which neglect snow hydrology.

Between-group variances for each set of parameterization options, divided by total ensemble variances and averaged over each winter, are given in Table 9. The largest fractions of variance in snow mass simulations are explained by choices of parameterizations for exchange coefficients (which determine the amount of melt due to sensible heat transfer during warm periods in winter) and liquid water retention (which determines the fate of melt water). Changes in snow depth between snowfall events is dominated by the compaction of cold snow for most of the winter in 2005–2006 and 2008–2009, but removal of snow by mid-winter melt events is more important and hence the choice of surface flux parameterization accounts for more variability in the warmer winters. Variance in albedo simulations is, not surprisingly, sensitive to choices of albedo parameterization, but choices for snow cover fraction also influence the area-average albedo for shallow snow, particularly in the low-snow winter of 2006–2007. Surface temperature simulations are strongly controlled by the surface flux parameterization.

6. Model evaluation

Figs. 10–13, used in the last section to show spread in simulations with the 1701 configurations of JIM, also show observations of snow mass, snow depth, daily effective albedo and daily average surface temperature. The simulations encompass almost all of the snow mass and depth observations. Most configurations underestimate the snow mass in 2006–2007, but configurations that fail to capture melt events in November 2007 and March 2008 retain positive biases and overestimate snow mass for some time thereafter. Snow depth is both underestimated by configurations that melt snow too early and overestimated by configurations that underestimate snow density. Some of the albedo measurements are higher than any of the simulations, but this may partly be due to the difficulty of keeping radiometers clear during heavy snowfall. The

Please cite this article in press as: Essery R et al. A comparison of 1701 snow models using observations from an alpine site. Adv Water Resour (2012), http://dx.doi.org/10.1016/j.advwatres.2012.07.013

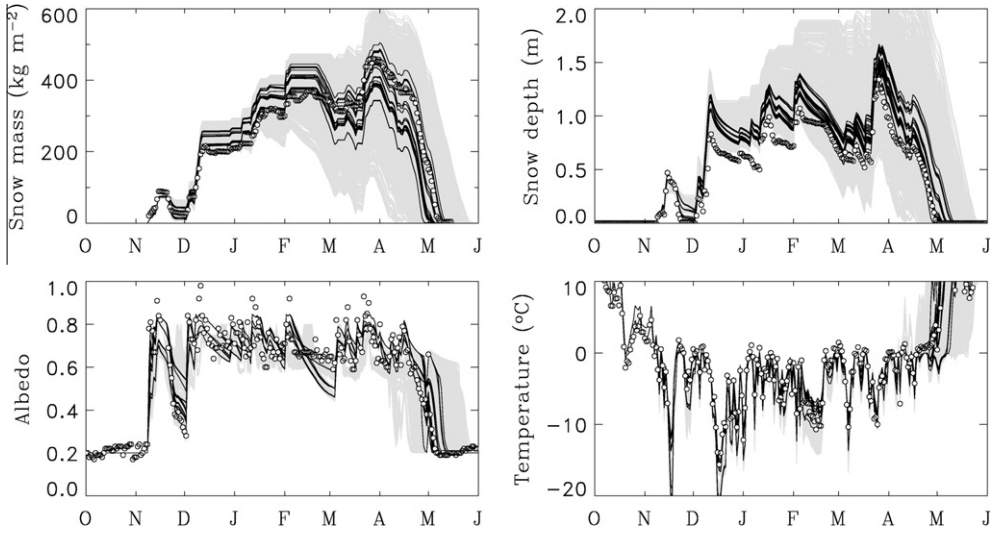

Fig. 12. As Fig. 10, but for 2007–2008.

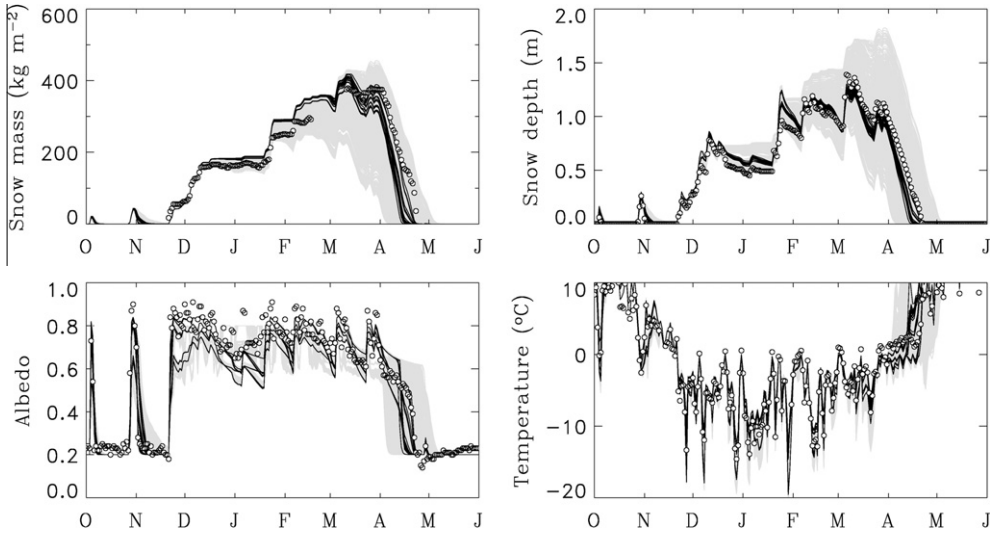

Fig. 13. As Fig. 10, but for 2008–2009.

largest cold biases in surface temperature simulations (up to 8 °C for daily averages and over 15 °C for some individual hours) are given by configurations using surface flux parameterization option 0 (which minimizes downwards heat transport from the atmosphere) and thermal conductivity parameterization option 1 (which minimizes upwards heat conduction in the snow).

Several metrics are commonly used to evaluate the performance of models in comparison with observations. Root mean square error is probably the most common and, simply referred to as "error", is used exclusively here (this, of course, is not purely a measure of model error but also integrates driving and evaluation data errors). To rank JIM configurations in their ability to simulate snow mass, errors for each winter were calculated for every configuration. Errors were normalized by the highest configuration error in each winter for comparison and ranked in order of increasing normalized errors; results are shown in Fig. 16. There is a group of 33 configurations, all of which use the least sophisticated albedo, surface flux and snow hydrology parameterizations, that have large errors for every winter. At the other extreme, there are several configurations that give consistently good performances with maximum errors roughly a third of those for the worst simulations. The best 49 configurations ranked in this way all use either the physical or empirical albedo parameterizations and one of the two snow hydrology parameterizations that can retain melt water, and none of them use the Monin–Obukhov surface flux parameterization. These are not, however, the configurations giving the lowest errors in individual winters; some configurations give low errors in one winter and high errors in another. The 16 configurations with the greatest inconsistencies between their best and worst snow mass simulations for the four winters all use options 0 for compaction and hydrology parameterizations and option 2 for albedo parameterization. In each case, these models give high normalized errors for 2006–2007, low errors for 2007–2008 and intermediate errors for the other two winters. Using only one winter of observations to select a model structure would run the risk of choosing a model that will not perform well in other winters.

Fig. 14 showed that the ensemble-mean snow mass compares well with observations in all winters except 2006–2007, but there are individual configurations with lower snow mass errors; in fact, there are 31 configurations which give lower snow mass errors than the ensemble mean in every winter. Correlations between series of daily snow mass errors for different configurations vary

Please cite this article in press as: Essery R et al. A comparison of 1701 snow models using observations from an alpine site. Adv Water Resour (2012), http://dx.doi.org/10.1016/j.advwatres.2012.07.013

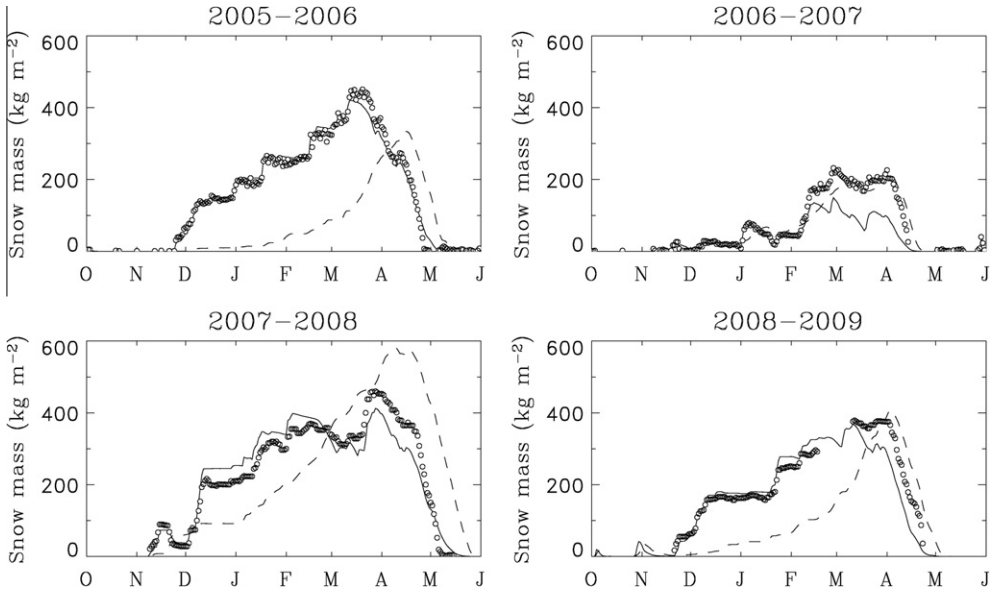

Fig. 14. Ensemble mean (solid lines) and spread (dashed lines) for snow mass simulations in each winter. Circles show snow mass observations.

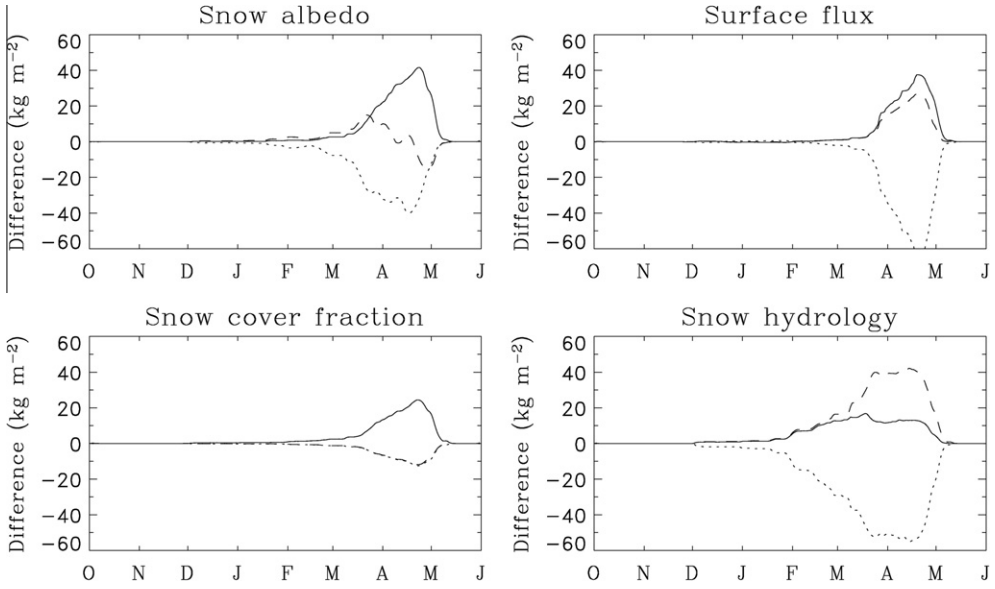

Fig. 15. Differences between 2005–2006 ensemble mean snow mass and group means for configurations using snow albedo, surface flux, snow cover fraction and snow hydrology parameterization options 0 (solid lines), 1 (dashed lines) and 2 (dotted lines).

greatly, from nearly 0 (e.g. between configurations 2010110 and 2010120 in 2005–2006) to nearly 1 (e.g. between configurations 2010110 and 2010111).

The numbers of times that each parameterization option is used in the 30 configurations with the lowest errors for each winter are shown by separate bar charts for snow mass, snow depth, albedo and surface temperature simulations in Fig. 17. Most of the best snow mass simulations use one of the hydrology options that can retain melt water. A constant snow density is not used in any of the best snow depth or temperature simulations and few of the best albedo simulations. The option of diagnosing snow albedo from temperature is not used in any of the best albedo simulations and few of the best snow mass or depth simulations. A constant exchange coefficient is only used in a few of the best snow mass simulations but the Monin–Obukhov surface flux parameterization is only used in a few of the best albedo and none of the best temperature simulations. Compared with the simulations of other variables, the choice of fresh snow density parameterization is most important for simulation of snow depth and the choice of snow thermal conductivity parameterization is most important for simulation of surface temperature.

No single configuration gives the best simulation for all evaluation variables and all winters. This is a ubiquitous situation in the multi-objective selection or calibration of hydrological models, and many studies have addressed the problem of optimization in the face of non-uniqueness. Without imposing any relative weighting of objectives, configurations can be rejected if *any* other configuration can be found with better performance for all objectives; the set of configurations remaining after rejection is "Pareto optimal". This approach has been widely used in hydrological modelling [38,52], but it turns out that the Pareto set of configurations minimizing the 16 error measures for simulation of four variables over

Please cite this article in press as: Essery R et al. A comparison of 1701 snow models using observations from an alpine site. Adv Water Resour (2012), http://dx.doi.org/10.1016/j.advwatres.2012.07.013

Table 9
Between-group variances divided by total ensemble variances and averaged over each winter for simulations of snow mass, snow depth, albedo and surface temperature for differing choices of parameterizations of (from left to right) snow compaction, fresh snow density, snow albedo, surface fluxes, snow cover fraction, snow hydrology and thermal conductivity. The largest values in each row are highlighted in bold.

	n_c	n_s	n_a	n_e	n_f	n_h	n_t
Snow mass							
2005–2006	0.03	0.01	0.10	0.11	0.03	**0.48**	0.03
2006–2007	0.01	<0.01	0.11	0.22	0.22	**0.25**	0.01
2007–2008	<0.01	<0.01	0.05	**0.49**	0.08	0.26	0.01
2008–2009	0.01	<0.01	0.07	0.16	0.10	**0.37**	0.03
Snow depth							
2005–2006	**0.75**	0.12	0.06	0.07	0.02	0.10	0.02
2006–2007	0.15	0.07	0.11	0.19	**0.20**	0.16	0.01
2007–2008	0.34	0.07	0.05	**0.39**	0.05	0.13	0.01
2008–2009	**0.58**	0.11	0.05	0.13	0.06	0.11	0.02
Albedo							
2005–2006	0.03	0.01	**0.47**	0.05	0.28	0.01	0.01
2006–2007	0.03	0.01	**0.32**	0.10	**0.32**	0.04	0.01
2007–2008	0.01	<0.01	**0.51**	0.11	0.20	0.01	<0.01
2008–2009	0.02	0.01	**0.40**	0.10	0.26	0.01	0.01
Surface temperature							
2005–2006	0.03	0.01	0.05	**0.60**	0.15	0.09	0.03
2006–2007	0.02	0.01	0.04	**0.63**	0.20	0.04	0.01
2007–2008	0.02	0.01	0.04	**0.62**	0.12	0.09	0.02
2008–2009	0.02	<0.01	0.04	**0.69**	0.12	0.05	0.02

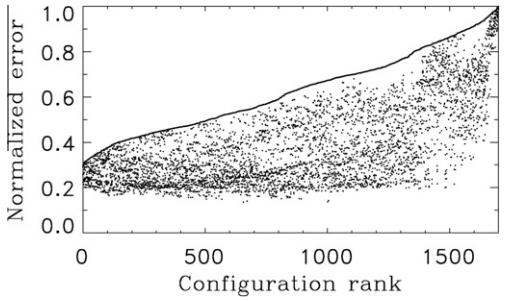

Fig. 16. Errors in snow mass simulations normalized by the largest error for each winter and ranked in order of largest normalized error for any winter.

four winters at Col de Porte is large (1242 members) and does not constrain the model ensemble much.

An alternative approach for multi-objective optimization, more akin to methods used for the assimilation of observations in meteorological models, is to define a single cost function summing squared differences between simulations and observations, multiplied by factors to weight and non-dimensionalize errors in different variables. Known observation error variances or subjective levels of importance could be used for the weighting factors. Using observations of four variables (snow mass, snow depth, albedo and surface temperature) over four winters, the cost function here is chosen to be

$$J = \sum_{i=1}^{4}\sum_{j=1}^{4}\sum_{k=1}^{N_{ij}} \frac{(v_{ijk}^{\mathrm{sim}} - v_{ijk}^{\mathrm{obs}})^2}{16 N_{ij} w_{ij}^2} - 1, \qquad (64)$$

where v^{obs} is an observation of a variable, v^{sim} is a simulated value of the same variable at the same time and the sums are over the winters (index i), the variables (index j) and the N_{ij} observations of variable j in winter i (index k). The w_{ij} weighting factors are set to the lowest simulation errors achieved by any configuration for each variable in each winter to give $J = 0$ for a configuration with the lowest errors in all cases, if such a configuration exists. In fact, the lowest value achieved is 1.87 for configuration number 320 (0102212). Simulations by configurations giving the 30 lowest values for the cost function are picked out from the ensembles by black lines in Figs. 10–13. As shown in Fig. 18, all of these configurations use the physical snow compaction parameterization, none of them uses the diagnosed snow albedo or the Monin–Obukhov surface flux parameterization, and none of them neglects snow hydrology. This subset does not necessarily include the simulation with the lowest error for a particular variable and winter, but it can be seen to give a compromise for reasonable simulations of most variables in most winters. For 2006–2007, the selected configurations match the measured snow depth well but underestimate the snow mass from mid-February onwards. In fact, the manual measurements of snow mass were also lower than the automatic measurements in that period. This highlights a difficulty with evaluating snow simulations against point measurements; snow properties can vary greatly over short distances, and relative differences are of greater significance for winters with shallow snow.

Even the more physically-based parameterizations of snow processes contain parameters with values that are not well constrained by observations or theory, and it is as easy to obtain poor model performance with poor choices of parameter values as it is with poor choices of model structure. Calibrating the parameters in a land surface model for global atmospheric modelling applications is not straightforward, but models are often calibrated for hydrological applications, and the organizers of intercomparison projects sometimes make a subset of the evaluation data available to allow a degree of model calibration. A full calibration of JIM has not been attempted, but configuration number 1700 (2022222), which performed poorly in the original simulations, has been calibrated by random sampling of the five parameters $\alpha_{\max}$, $\alpha_{\min}$, d_0, T_c and z_0 to minimize the cost function for 2006–2007. Errors for snow mass, snow depth, albedo and surface temperature are given in Table 10 for the uncalibrated and calibrated configuration, compared with errors for configuration number 849 (1011110) which performed well without calibration. Errors for the poorly performing configuration are greatly reduced by calibration, but the overall performance of a configuration that performs well without calibration is not matched.

7. Conclusions and discussion

The snow model presented here, built entirely from process parameterizations in common use, generates ensembles that span the range of results produced by existing models for the SnowMIP sites and gives similar wide ranges for new simulations at Col de Porte. Many of the conclusions drawn from comparisons of the simulations with observations match those from earlier model intercomparison projects but are demonstrated with much greater clarity. Failure to predict early and mid-winter melt events accurately can lead to persistent errors, so prediction is more challenging for warmer winters. There is no "best" model, and increasing model complexity beyond some minimum requirements is no guarantee of improved model performance; well-established empirical parameterizations often give results that are as good as more physically-based parameterizations. Some models, however, give results that are consistently amongst the best, and some models have consistently poor performance. Many models give inconsistent results and so cannot be considered to be "good" models, even if they give good results in some winters. Evaluations of snow mass, snow depth, albedo and surface temperature simulations, either separately or combined in a single measure of model performance, show that the best results are given by models with prognostic representations of snow albedo and density. For a site such as Col de Porte which has deep snow but can have surface melting

Please cite this article in press as: Essery R et al. A comparison of 1701 snow models using observations from an alpine site. Adv Water Resour (2012), http://dx.doi.org/10.1016/j.advwatres.2012.07.013

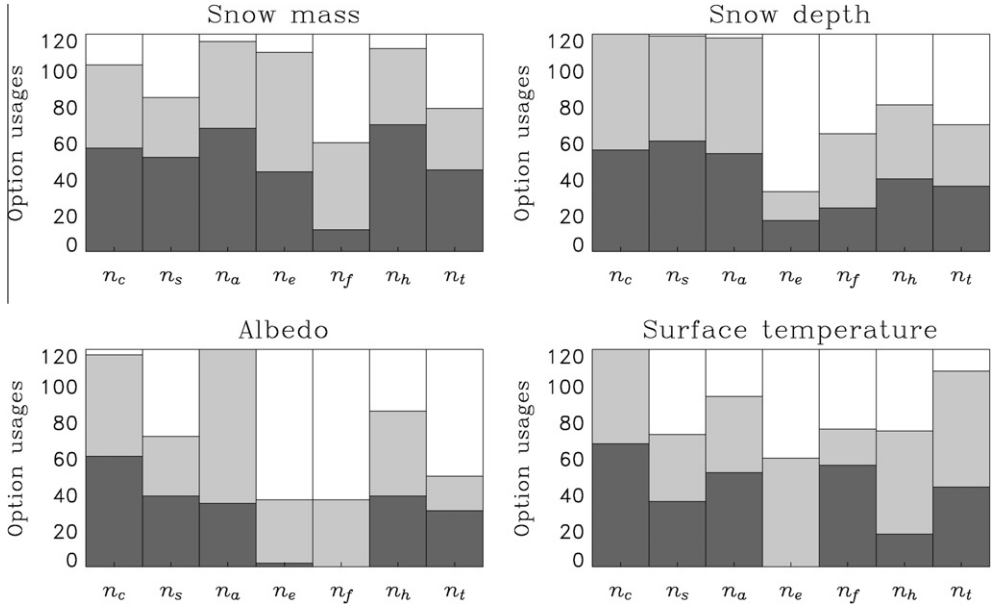

Fig. 17. Numbers of times that parameterization options are used in the 30 configurations with the lowest errors for snow mass, snow depth, albedo and surface temperature simulations for each of four winters. The bars are, from left to right, for snow compaction, fresh snow density, snow albedo, surface flux, snow cover fraction, snow hydrology and thermal conductivity parameterizations. Dark grey bars are for option 0, light grey for option 1 and white for option 2.

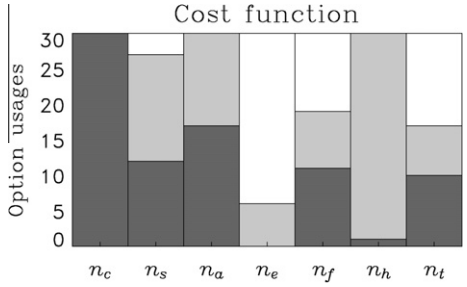

Fig. 18. As Fig. 17, but for the numbers of times that parameterization options are used in configurations giving the 30 lowest values for a cost function combining errors in snow mass, snow depth, albedo and surface temperature simulations for all four winters.

Table 10
Errors for calibrated and uncalibrated 2006–2007 simulations.

Configuration	Snow mass (kg m^{-2})	Snow depth (m)	Albedo	Surface temperature (°C)
1700 uncalibrated	77	0.12	0.13	3.8
1700 calibrated	35	0.07	0.13	2.4
849 uncalibrated	23	0.08	0.08	1.7

at any time in the winter, it is important to have at least a simple representation of liquid water storage and refreezing in the snow. Using a turbulent flux parameterization that decouples the surface from the atmosphere in strongly stable situations can lead to poor simulations; better results were obtained by using a constant surface exchange coefficient, but it should be noted that this parameter was previously calibrated for Col de Porte. Choices for parameterizations of fresh snow density and thermal conductivity appear to be less critical for simulation of the snow properties evaluated here, but they will be important for other applications; it is important to know if a low density surface layer is preserved after burial for avalanche risk assessment, for example, and thermal conductivity is important for the prediction of soil temperatures under snow.

As has often been found in simulations of hydrological variables, the ensemble-mean snow mass compares well with observations but there are individual ensemble members with consistently better performances. Calculation of sample statistics from ensemble simulations with equal weighting assumes that the ensemble members are all independent and equally plausible. The ensemble used here was constructed to explore the range of behaviours produced by current snow models rather than with the aim of quantifying uncertainty in predictions made with the best of these models; some of the parameterizations used were expected to give poor results based on previous evaluations, and some of the ensemble members were found to be highly correlated.

Calibration of models by adjustment of parameters to improve performance metrics for a calibration period, followed by testing on independent data, is common, particularly in hydrology. Errors in model structure can be compensated by calibration to some degree, so parameter uncertainty and structural uncertainty are related. For a complex model with many parameters, there is a danger of over-fitting the model to the calibration data and hence reducing its predictive ability. Several model selection criteria have been developed that use measures of model complexity and performance in evaluation after calibration [24]. All of the parameter values used in JIM are taken from literature sources, and little attempt has been made to calibrate them so far. Calibration of such a large ensemble will be an interesting computational challenge, even using efficient optimization algorithms (e.g. [102,106]); more than thirty thousand parameter values would have to be selected if every configuration were to be calibrated independently. Calibration of a subset of parameters or a subset of configurations selected to span the uncalibrated ensemble could be attempted first.

The relative importance of different snow process parameterizations will vary with climate, so JIM will be tested at other sites. The use of driving data from well-instrumented sites such as Col de Porte, here and in many other studies, allows highly controlled evaluations of model performance but does not reflect how models are actually used in practical applications. Models often have to be run on the large scales of catchments or climate model grid cells, and they are often coupled to atmospheric models that provide biased driving data and respond to errors in predicted surface

Please cite this article in press as: Essery R et al. A comparison of 1701 snow models using observations from an alpine site. Adv Water Resour (2012), http://dx.doi.org/10.1016/j.advwatres.2012.07.013

fluxes, generating feedbacks. Evaluations of snow models in the applications for which they are intended, such as Dutra et al. [35], are to be encouraged.

Acknowledgements

This work was partly supported by NERC grant NE/H008187/1 and ESA ESTEC contract 23103/09/NL/JC. Thanks are expressed to the CNRM-GAME/CEN staff who have contributed to the collection, collation and archiving of Col de Porte data over many years. We also thank EDF-DTG for collaboration on SWE and precipitation measurements and Martyn Clark for his detailed and helpful review of this paper.

References

[1] Albert M, Krajeski G. A fast, physically based point snowmelt model for use in distributed applications. Hydrol Processes 1998;12:1809–24.
[2] Albert M, Koh G, Perron F. Radar investigations of melt pathways in a natural snowpack. Hydrol Processes 1999;13:2991–3000.
[3] Anderson EA. A point energy and mass balance model of a snow cover. NOAA Technical Report NWS 19, Office of Hydrology, National Weather Service, 1976.
[4] Andreadis KM, Storck P, Lettenmaier DP. Modeling snow accumulation and ablation processes in forested environments. Water Resour Res 2009;45. http://dx.doi.org/10.1029/2008WR007042.
[5] Andreas EL. Parameterizing scalar transfer over snow and ice: a review. J Hydrometeorol 2002;3:417–32.
[6] Bartelt P, Lehning M. A physical SNOWPACK model for the Swiss avalanche warning: Part I: numerical model. Cold Reg Sci Technol 2002;35:123–45.
[7] Bartlett PA, MacKay MD, Verseghy DL. Modified snow algorithms in the Canadian land surface scheme: model runs and sensitivity analysis at three boreal forest stands. Atmos-Ocean 2006;44:207–22.
[8] Best MJ et al. The Joint UK Land Environment Simulator (JULES), model description. Part 1: energy and water fluxes. Geosci Model Dev 2011;4:677–99.
[9] Bohn TJ, Sonessa MY, Lettenmaier DP. Seasonal hydrologic forecasting: do multi-model ensemble averages always yield improvements in forecast skill? J Hydrometeorol 2010;11:1358–72.
[10] Boone A, Etchevers P. An intercomparison of three snow schemes of varying complexity coupled to the same land surface model: local-scale evaluation at an alpine site. J Hydrometeorol 2001;2:374–94.
[11] Boone A. Description du schema de neige ISBA-ES (Explicit Snow). Centre National de Recherches Météorologiques, Météo-France, Toulouse, 2002. Available from: http://www.cnrm.meteo.fr/IMG/pdf/snowdoc.pdf.
[12] Boone A et al. The Rhône-aggregation land surface scheme intercomparison project: an overview. J Clim 2004;17:187–208.
[13] Bowling LC et al. Simulation of high latitude hydrological processes in the Torne-Kalix basin: PILPS Phase 2e. 1: experiment design and summary intercomparisons. Global Planet Change 2003;38:1–30.
[14] Brasnett B. A global analysis of snow depth for numerical weather prediction. J Appl Meteorol 1999;38:726–40.
[15] Brown R, Bartlett P, MacKay M, Verseghy D. Evaluation of snow cover in CLASS for SnowMIP. Atmos-Ocean 2006;44:223–38.
[16] Brun E, David P, Sudul M, Brunot G. A numerical model to simulate snow-cover stratigraphy for operational avalanche forecasting. J Glaciol 1992;38:13–22.
[17] Calonne N, Flin F, Morin S, Lesaffre B, Rolland du Roscoat S, Geindreau C. Numerical and experimental investigations of the effective thermal conductivity of snow. Geophys Res Lett 2011;38. http://dx.doi.org/10.1029/2011GL049234.
[18] Clark MP, Slater AG, Rupp DE, Woods RA, Vrugt JA, Gupta HV, et al. Framework for Understanding Structural Errors (FUSE): a modular framework to diagnose differences between hydrological models. Water Resour Res 2008;44. http://dx.doi.org/10.1029/2007WR006735.
[19] Clark MP, Kavetski D. Ancient numerical daemons of conceptual hydrological modelling: 1. Fidelity and efficiency of time stepping schemes. Water Resour Res 2010;46. http://dx.doi.org/10.1029/2009WR008894.
[20] Clark MP, Kavetski D, Fenicia F. Pursuing the method of multiple working hypotheses for hydrological modeling. Water Resour Res 2011;47. http://dx.doi.org/10.1029/2010WR009827.
[21] Clark MP, Hendrikx J, Slater AG, Kavetski D, Anderson B, Cullen NJ, et al. Representing spatial variability of snow water equivalent in hydrologic and land-surface models: a review. Water Resour Res 2011;47. http://dx.doi.org/10.1029/2011WR010745.
[22] Colbeck S. Theory of water percolation in snow. J Glaciol 1972;11:369–85.
[23] Cox PM, Betts RA, Bunton C, Essery RLH, Rowntree PR, Smith J. The impact of new land surface physics on the GCM simulation of climate and climate sensitivity. Clim Dyn 1999;15:183–203.
[24] Cox GM, Gibbons JM, Wood ATA, Craigon J, Ramsden SJ, Crout NMJ. Towards the systematic simplification of mechanistic models. Ecol Mod 2006;198:240–6.
[25] Crank J, Nicolson P. A practical method for numerical evaluation of solutions of partial differential equations of the heat conduction type. Proc Cambridge Philos Soc 1947;43:50–67.
[26] Dai Y, Zeng Q. A land surface model (IAP94) for climate studies. Part I: formulation and validation in off-line experiments. Adv Atmos Sci 1997;14:433–60.
[27] Derbyshire SH. Boundary-layer decoupling over cold surfaces as a physical boundary-instability. Bound-Layer Meteor 1999;90:297–325.
[28] Deutsches Klimarechenzentrum (DKRZ) Modellbetreuungsgruppe. The ECHAM3 atmospheric general circulation model. DKRZ Technical Report No. 6, ISSN 0940-9237, Deutsches Klimarechenzentrum, Hamburg, Germany, 1992.
[29] Dickinson RE, Henderson-Sellers A, Kennedy PJ. Biosphere-Atmosphere Transfer Scheme (BATS) version 1e as coupled to the NCAR Community Climate Model. NCAR Technical Note NCAR/TN-387+STR; National Center for Atmospheric Research, Boulder, CO., 1993.
[30] Dirmeyer PA, Gao X, Zhao M, Guo Z, Oki T, Hanasaki N. GSWP-2: multimodel analysis and implications for our perception of the land surface. Bull Am Meteorol Soc 2009;87:1381–97.
[31] Donald JR, Soulis ED, Kouwen N, Pietroniro A. A land cover-based snow cover representation for distributed hydrologic models. Water Resour Res 1995;31:995–1009.
[32] Douville H, Royer JF, Mahfouf JF. A new snow parameterization for the Meteo-France climate model. Part I: validation in stand-alone experiments. Clim Dyn 1995;12:21–35.
[33] Drusch M, Vasiljevic D, Viterbo P. ECMWF's global snow analysis: assessment and revision based on satellite observations. J Appl Meteorol 2004;43:1282–94.
[34] Dutra E, Balsamo G, Viterbo P, Miranda PMA, Beljaars A, Schär C, et al. An improved snow scheme for the ECMWF land surface model: description and offline validation. J Hydrometeorol 2010;11:899–916.
[35] Dutra E, Viterbo P, Miranda PMA, Balsamo G. Complexity of snow schemes in a climate model and its impact on surface energy and hydrology. J Hydrometeorol 2011. http://dx.doi.org/10.1175/JHM-D-11-072.1.
[36] Essery R, Martin E, Douville H, Fernández A, Brun E. A comparison of four snow models using observations from an alpine site. Clim Dyn 1999;15:583–93.
[37] Essery R, Li L, Pomeroy J. A distributed model of blowing snow over complex terrain. Hydrol Processes 1999;13:2423–38.
[38] Essery R, Etchevers P. Parameter sensitivity in simulations of snowmelt. J Geophys Res 2004;109. http://dx.doi.org/10.1029/2004JD005036.
[39] Essery R, Pomeroy J. Implications of spatial distributions of snow mass and melt rate for snow-cover depletion: Theoretical considerations. Ann Glaciol 2004;38:261–5.
[40] Essery RLH, Blyth EM, Harding RJ, Lloyd CM. Modelling albedo and distributed snowmelt across a low hill on Svalbard. Nordic Hydrol 2005;36:207–18.
[41] Essery R, Rutter N, Pomeroy J, Baxter R, Stähli M, Gustafsson D, et al. SnowMIP2: an evaluation of forest snow process simulations. Bull Am Meteorol Soc 2009;90. http://dx.doi.org/10.1175/2009BAMS2629.1.
[42] Etchevers P et al. Validation of the surface energy budget simulated by several snow models. Ann Glaciol 2004;38:150–8.
[43] Fassnacht SR, Soulis ED. Implications during transitional periods of improvements to the snow processes in the land surface scheme – hydrological model WATCLASS. Atmos-Ocean 2002;40:389–403.
[44] Feng X, Sahoo A, Arsenault K, Houser P, Luo P, Troy TJ. The impact of snow model complexity at three CLPX sites. J Hydrometeorol 2008;9:1464–81.
[45] Flanner MG, Zender CS. Snowpack radiative heating: influence on Tibetan Plateau climate. Geophys Res Lett 2005;32. http://dx.doi.org/10.1029/2004GL022076.
[46] Flanner MG, Zender CS. Linking snowpack microphysics and albedo evolution. J Geophys Res 2006;111. http://dx.doi.org/10.1029/2005JD006834.
[47] Forland E, Allerup P, Dahlström B, Elomaa ET, Perälä J, Rissanen P, Vedin H, Vejen F. Manual for operational correction of Nordic precipitation data. Tech. rep., Det Norske Meteorologiske Institutt 1996.
[48] Franz KJ, Butcher P, Ajami NK. Addressing snow model uncertainty for hydrologic prediction. Adv Water Resour 2010;33:820–32.
[49] Frei A, Miller JA, Robinson DA. Improved simulations of snow extent in the second phase of the Atmospheric Model Intercomparison Project (AMIP-2). J Geophys Res 2003;108. http://dx.doi.org/10.1029/2002JD003030.
[50] Green RO, Dozier J, Roberts D, Painter T. Spectral snow-reflectance models for grain-size and liquid water fraction in melting snow for the solar-reflected spectrum. Ann Glaciol 2002;34:71–3.
[51] Guo Z, Dirmeyer PA, Gao X, Zhao M. Improving the quality of simulated soil moisture with a multi-model ensemble approach. Quart J Roy Meteor Soc 2007;133:731–47.
[52] Gupta HV, Sorooshian S, Yapo PO. Toward improved calibration of hydrologic models: multiple and noncomensurable measures of information. Water Resour Res 1998;34:751–63.
[53] Gusev YM, Nasonova ON. The land surface parameterization scheme SWAP: description and partial validation. Global Planet Change 1998;19:63–86.
[54] Gustafsson D, Waldner PA, Stähli M. Factors governing the formation and persistence of layers in a subalpine snowpack. Hydrol Processes 2004;18:1165–83.

Please cite this article in press as: Essery R et al. A comparison of 1701 snow models using observations from an alpine site. Adv Water Resour (2012), http://dx.doi.org/10.1016/j.advwatres.2012.07.013

[55] Haddeland I et al. Multimodel estimate of the global terrestrial water balance: setup and first results. J Hydrometeorol 2011;12. http://dx.doi.org/10.1175/2011JHM1324.1.
[56] Hedstrom NR, Pomeroy JW. Measurement and modelling of snow interception in the boreal forest. Hydrol Processes 1998;12:1611–25.
[57] Helgason W, Pomeroy J. Characteristics of the near-surface boundary layer within a mountain valley during winter. J Appl Meteor Climatol 2011. http://dx.doi.org/10.1175/JAMC-D-11-058.1.
[58] Hirashima H, Yamaguchi S, Sati A, Lehning M. Numerical modeling of liquid water movement through layered snow based on new measurements of the water retention curve. Cold Reg Sci Technol 2010;64:94–103.
[59] Jin J, Gao X, Yang ZL, Bales RC, Sorooshian S, Dickinson RE, et al. Comparative analyses of physically based snowmelt models for climate simulations. J Clim 1999;12:2643–57.
[60] Jordan R. A one-dimensional temperature model for a snow cover. Technical documentation for SNTHERM.89. CRREL Special Report 91-16; US Army Core of Engineers Cold Regions Research and Engineering Laboratory, Hanover, NH, 1991.
[61] Kodama M. Continuous monitoring of snow water equivalent using cosmic ray neutrons. Cold Reg Sci Technol 1980;3:295–303.
[62] Kokhanovsky AA, Zege EP. Scattering optics of snow. Appl Opt 2004;43:1589–602.
[63] Lehning M, Bartelt P, Brown B, Fierz C, Satyawali P. A physical SNOWPACK model for the Swiss avalanche warning Part II: snow microstructure. Cold Reg Sci Technol 2002;35:147–67.
[64] Lehning M, Volksch I, Gustafsson D, Nguyen TA, Stähli M, Zappa M. ALPINE3D: a detailed model of mountain surface processes and its application to snow hydrology. Hydrol Processes 2006;20:2111–28.
[65] Liston GE, Sturm M. A snow-transport model for complex terrain. J Glaciol 1998;44:498–516.
[66] Liston GE. Representing subgrid snow cover heterogeneities in regional and global models. J Clim 2004;17:1381–97.
[67] Louis JF. A parametric model of vertical eddy fluxes in the atmosphere. Bound-Layer Meteor 1979;17:187–202.
[68] Lynch-Stieglitz M. The development and validation of a simple snow model for the GISS GCM. J Clim 1994;7:1842–55.
[69] Marks D, Dozier J. Climate and energy exchange at the snow surface in the alpine region of the Sierra Nevada. 2. Snow cover energy balance. Water Resour Res 1992;28:3043–54.
[70] Marks D, Kimball J, Tingey D, Link T. The sensitivity of snowmelt processes to climate conditions and forest cover during rain-on-snow: a study of the 1996 Pacific Northwest flood. Hydrol Processes 1998;12:1569–87.
[71] Marshall S, Oglesby R. An improved snow hydrology for GCMs. Part 1: snow cover fraction, albedo, grain size, and age. Clim Dyn 1994;10:21–37.
[72] Marshall SE, Warren SG. Parameterization of snow albedo for climate models. In: Goodison BE, Barry RG, Dozier J, editors. Large scale effects of seasonal snow cover. IAHS Publications; 1987. p. 166.
[73] Martin E, Lejeune Y. Turbulent fluxes above the snow surface. Ann Glaciol 1998;26:179–83.
[74] Morin S, Lejeune Y, Lesaffre B, Panel JM, Poncet D, David P, et al. A 18-year long (1993–2011) snow and meteorological dataset from a mid-altitude mountain site (Col de Porte, France, 1325 m alt.) for driving and evaluating snowpack models. Earth Syst Sci Data 2012;4. http://dx.doi.org/10.5194/essd-4-13-2012.
[75] Mott R, Schirmer M, Bavay M, Grünewald T, Lehning M. Understanding snow-transport processes shaping the mountain snow-cover. The Cryosphere 2010;4. http://dx.doi.org/10.5194/tc-4-545-2010.
[76] Nijssen B et al. Simulation of high latitude hydrological processes in the Torne–Kalix basin: PILPS Phase 2(e). 2: comparison of model results with observations. Global Planet Change 2003;38:31–53.
[77] Niu GY, Yang ZL. An observation-based formulation of snow cover fraction and its evaluation over large North American river basins. J Geophys Res 2007;112. http://dx.doi.org/10.1029/2007JD008674.
[78] Niu GY et al. The community Noah land surface model with multiparameterization options (Noah-MP): 1. Model description and evaluation with local-scale measurements. J Geophys Res 2011;116. http://dx.doi.org/10.1029/2010JD015139.
[79] Oke TR. Boundary layer climates. Routledge; 1987.
[80] Oleson KW, et al. Technical description of the Community Land Model (CLM). NCAR Technical Note NCAR/TN-461+STR; National Center for Atmospheric Research, Boulder, CO., 2004.
[81] Oleson KW, et al. Technical description of version 4.0 of the Community Land Model (CLM). NCAR Technical Note NCAR/TN-478+STR; National Center for Atmospheric Research, Boulder, CO., 2010.
[82] Paquet E, Laval MT. Operation feedback and prospects of EDF Cosmic-Ray Snow Sensors. La Houille Blanche 2006;2. http://dx.doi.org/10.1051/lhb:200602015.
[83] Pedersen CA, Winther JG. Intercomparison and validation of snow albedo parameterization schemes in climate models. Clim Dyn 2005;25:351–62.
[84] Pitman AJ, Xia Y, Leplastrier M, Henderson-Sellers A. The CHAmeleon Surface Model: description and use with the PILPS phase 2(e) forcing data. Global Planet Change 2003;38:121–35.
[85] Pomeroy JW, Gray DM, Brown T, Hedstrom NR, Quinton WL, Granger RJ, et al. The cold regions hydrological model: a platform for basing model structure on physical evidence. Hydrol Processes 2007;19:2650–67.
[86] Randall DA et al. The greening of the Colorado State University general circulation model. J Clim 1996;9:738–63.
[87] Roebber PJ, Bruening SL, Schultz DM, Cortinas JV. Improving snowfall forecasting by diagnosing snow density. Wea Forecasting 2002;18:264–87.
[88] Roesch AH, Gilgen M, Wild M, Ohmura A. A new snow cover fraction parameterization for the ECHAM4 GCM. Clim Dyn 2001;17:933–45.
[89] Roesch A. Evaluation of surface albedo and snow cover in AR4 coupled climate models. J Geophys Res 2006;111. http://dx.doi.org/10.1029/2005JD006473.
[90] Rutter N et al. Evaluation of forest snow processes models (SnowMIP2). J Geophys Res 2009;114. http://dx.doi.org/10.1029/2008JD011063.
[91] Schlosser CA et al. Simulations of a boreal grassland hydrology at Valdai, Russia: PILPS Phase 2(d). Mon Wea Rev 2000;128:301–21.
[92] Sellers PJ, Randall DA, Collatz GJ, Berry JA, Field CB, Dazlich DA, et al. A revised land surface parameterization (SiB2) for atmospheric GCMs. 1. Model formulation. J Clim 1996;9:676–705.
[93] Shmakin AB. The updated version of SPONSOR land surface scheme: PILPS-influenced improvements. Global Planet Change 1998;19:49–62.
[94] Slater AG, Pitman AJ, Desborough CE. The validation of a snow parameterization designed for use in general circulation models. Int J Climatol 1998;18:595–617.
[95] Slater AG et al. The representation of snow in land surface schemes: results from PILPS 2(d). J Hydrometeorol 2001;2:7–25.
[96] Smirnova TG, Brown JM, Benjamin SG, Kim D. Parameterization of cold-season processes in the MAPS land-surface scheme. J Geophys Res 2000;105:4077–86.
[97] Strasser U, Etchevers P, Lejeune Y. Inter-comparison of two snow models with different complexity using data from an alpine site. Nordic Hydrol 2002;33:15–26.
[98] Sturm M, Holmgren J, Konig M, Morris K. The thermal conductivity of seasonal snow. J Glaciol 1997;43:26–41.
[99] Sun S, Jin J, Xue Y. A simple snow-atmosphere-soil transfer model. J Geophys Res 1999;104:19587–97.
[100] Sun S, Xue Y. Implementing a new snow scheme in Simplified Simple Biosphere Model. Adv Atmos Sci 2001;18:335–54.
[101] Takata K, Emori S, Watanabe T. Development of the minimal advanced treatments of surface interaction and runoff. Global Planet Change 2003;38:209–22.
[102] Tolson BA, Shoemaker CA. Dynamically dimensioned search algorithm for computationally efficient watershed model calibration. Water Resour Res 2007;43. http://dx.doi.org/10.1029/2005WR004723.
[103] Truffaut F. Jules et Jim. Les Films du Carrosse, 1962.
[104] Verseghy DL. CLASS – a Canadian land-surface scheme for GCMs. I. Soil model. Int J Climatol 1991;11:111–33.
[105] Vionnet V, Brun E, Morin S, Boone A, Faroux S, Le Moigne P, et al. The detailed snowpack scheme Crocus and its implementation in SURFEX v7. Geosci Model Dev 2012;5. http://dx.doi.org/10.5194/gmd-5-773-2012.
[106] Vrugt JA, Gupta HV, Bouten W, Sorooshian S. A shuffled complex evolution metropolis algorithm for optimization and uncertainty assessment of hydrologic model parameters. Water Resour Res 2003;39:1201–14.
[107] Wang Z, Zeng X. Evaluation of snow albedo in land models for weather and climate studies. J Appl Meteor Climatol 2010;49:363–80.
[108] Wiscombe WJ, Warren SG. A model for the spectral albedo of snow. I: pure snow. J Atmos Sci 1980;37:2712–33.
[109] Xue Y, Sellers PJ, Kinter JL, Shukla J. A simplified biosphere model for global climate studies. J Clim 1991;4:345–64.
[110] Xue YK, Sun SF, Kahan DS, Jiao YJ. Impact of parameterizations in snow physics and interface processes on the simulation of snow cover and runoff at several cold region sites. J Geophys Res 2003;108. http://dx.doi.org/10.1029/2002JD003174.
[111] Yang ZL, Dickinson RE, Robock A, Vinnikov KY. Validation of the snow sub-model of the biosphere-atmosphere transfer scheme with Russian snow cover and meteorological observational data. J Clim 1997;10:353–73.
[112] Yang ZL, Niu GY. The versatile integrator of surface and atmosphere processes. Part 1. Model description. Global Planet Change 2003;38:175–89.
[113] Yen YC. Review of thermal properties of snow, ice and sea ice. CRREL Report 81-10; US Army Core of Engineers Cold Regions Research and Engineering Laboratory, Hanover, NH, 1981.
[114] Zeng X, Zhao M, Dickinson RE. Intercomparison of bulk aerodynamic algorithms for the computation of sea surface fluxes using the TOGA COARE and TAO data. J Clim 1998;11:2628–44.

Please cite this article in press as: Essery R et al. A comparison of 1701 snow models using observations from an alpine site. Adv Water Resour (2012), http://dx.doi.org/10.1016/j.advwatres.2012.07.013